Journal of Energy Storage 123 (2025) 116659

Contents lists available at ScienceDirect

Journal of Energy Storage

journal homepage: www.elsevier.com/locate/est

Research papers

The enhancement of metal hydride hydrogen storage performance using novel triple-branched fin

Puchanee Larpruenrudee [a,*], Nick S. Bennett [a], Robert Fitch [a], Emilie Sauret [b], YuanTong Gu [b], M.J. Hossain [c], Mohammad S. Islam [a]

[a] School of Mechanical and Mechatronic Engineering, University of Technology Sydney, 15 Broadway, Ultimo, NSW 2007, Australia
[b] School of Mechanical, Medical and Process Engineering, Faculty of Engineering, Queensland University of Technology, Brisbane, QLD 4000, Australia
[c] School of Electrical and Data Engineering, University of Technology Sydney, 15 Broadway, Ultimo, NSW 2007, Australia

ARTICLE INFO

Keywords:
Fins
Hydrogen absorption
Hydrogen desorption
Reaction time
Triple-branched fin
Y-shaped fin

ABSTRACT

The advantages of a high storage capacity and safety of metal hydride hydrogen storage (MHHS) have widely attracted people's interest in hydrogen storage. The improvement of the heat transfer performance is one of the key parameters to improve the overall MHHS performance. Various heat exchangers with complex structures have been developed for this purpose. However, the drawback of these heat exchangers is huge pressure losses. Therefore, this study aims to enhance the MHHS performance by considering the heat transfer improvement and maintaining the pressure loss inside the heat exchanger. To fulfil the requirement of heat transfer efficiency instead of using complex heat exchangers, a novel triple-branched fin is designed to attach to the simple straight tube heat exchanger. The effect of pressure losses due to the complex heat exchangers is analysed and compared with the simple straight tube. The novel fin heat exchanger's performance is also compared to conventional fins. Moreover, an enhancement of the novel fin geometries is considered with the parametric studies to achieve superior MHHS performance. The results indicate that the pressure losses are reduced by 31 % when using the straight tube instead of other complex heat exchangers. The novel triple-branched fin obtains the best heat transfer performance compared to other fin designs, including the quadrilateral fin and Y-shaped fin. After the geometrical enhancement of this novel fin, the duration of the absorption-desorption cycle is reduced by 25 % compared to the quadrilateral fin. Under the parametric study, heat transfer fluid temperature significantly affects the desorption process, while the heat transfer coefficient greatly affects the absorption process.

1. Introduction

The fin heat exchanger has been widely used for several engineering applications, such as thermal energy storage. The fin material with a high thermal conductivity is the key factor to increase the heat transfer rate. The main advantage of using fins as a heat exchanger is the simple installation and less maintenance during use, compared to other heat exchanger types [1]. For these purposes, several fin designs have been proposed for thermal energy storage with a cylindrical enclosure. Various fin parameters were considered for the radial fin design and optimisation. These included the fin thickness, fin height, fin number, fin length, fin width, and fin angle. The results from these fin parameters proved that increasing the fin number, height, and thickness improved the heat transfer performance by 20–23 % enhancement of phase change duration [2]. Similarly, increasing the fin numbers and fin width reduces the discharging time [3]. Beyond radial fins and annular fins, some studies also focused on heat transfer improvement based on the fin shape. These included the Y-shaped fin [4,5], V-shaped fins [6], and tree-shaped fins [7]. From these fins, the V-shaped fin obtained better heat transfer improvement, compared to the simple radial fin and annular fin. The enhancement of phase change duration by using a V-shaped fin was 82 %, while there were 74 % and 72 % enhancements of the phase change duration by using an annular fin and radial fin, compared to the case without fins [6]. For a Y-shaped fin, using this fin enhanced phase change duration by 81 %, compared to the case without fins [4]. Increasing the length of the Y-shaped fin boosted thermal penetration in the storage medium with a 16.5 % enhancement of the phase change duration [8]. From all fin designs, fin space had a favourable effect on the phase change duration for both the charging and discharging processes [1]. The fin number and fin length had a favourable effect on system performance rather than fin thickness [1].

* Corresponding author.
E-mail address: puchanee.larpruenrudee@uts.edu.au (P. Larpruenrudee).

https://doi.org/10.1016/j.est.2025.116659
Received 24 October 2024; Received in revised form 26 February 2025; Accepted 13 April 2025
Available online 26 April 2025

Nomenclature

C	reaction rate constant, s^{-1}
C_f	skin friction coefficient
C_p	specific heat, J kg^{-1} K^{-1}
c	maximum mass content of hydrogen in the metal, wt%
d	diameter of heat exchanger tube, m
E	activation energy, J mol^{-1}
H	fin height, mm
H_1	fin height for triple-branched section, m
h_f	heat transfer coefficient, W m^{-2} K^{-1}
K	permeability, m^2
L	length of Y-shaped fin, m
L_{HTF}	length of internal straight tube, m
L_1	fin width at the top branch, m
M	molecular weight, kg mol^{-1}
Nu	Nusselt number
P	pressure, MPa
P_0	hydrogen exerting pressure, MPa
Pr	Prandtl number
R	universal gas constant, J K^{-1} mol^{-1}
Re	Reynolds number
T	temperature, K
t	time, s
U	free-stream velocity at inlet, m s^{-1}
v	velocity, m s^{-1}
W	fin width, m
W_1	fin thickness at side branches, m
W_2	fin thickness at the middle branch, m
X	amount of hydrogen absorption/desorption, wt%
ΔH	reaction heat, J mol^{-1}
ΔS	reaction entropy, J mol^{-1} K^{-1}

Greek

ε	porosity
ρ	density, kg m^{-3}
μ	dynamic viscosity, Pa s
α	fin angle, °
τ_ω	wall shear stress, Pa
λ	thermal conductivity, W m^{-1} K^{-1}

Subscript

0	initial or exerting condition
abs	ambient or absorption
b	middle branch fin of the triple-branched fin section
des	desorption
e	effective
eq	equilibrium
f	fluid
H_2	hydrogen
max	maximum
ref	reference
ss	saturated
y	Y-shaped fin section

Abbreviation

MH	metal hydride
MHHS	metal hydride hydrogen storage
HTF	heat transfer fluid
HCHE	helical coil heat exchanger
SCHE	semi-cylindrical coil heat exchanger
SCHE-CR	semi-cylindrical coil heat exchanger with central return tube
STHE	straight tube heat exchanger

For the metal hydride hydrogen storage (MHHS), MHHS is a solid hydrogen storage technique that has recently attracted researcher interest due to its advantages that offer a high hydrogen capacity and high safety [9,10]. However, the main disadvantage of this technique is the low thermal conductivity of the metal hydride (MH) materials, which negatively affects the hydrogen kinetic reaction [11]. The enhancement of the heat transfer performance inside the MHHS is a key method to improve the hydrogen kinetic reaction rate. For this purpose, several heat exchangers have been used for heat transfer enhancement. Using fins as the internal heat exchanger is also another technique to improve heat transfer performance under the consideration of natural convection conditions [12,13]. The fin arrangement also results in a more uniform temperature distribution inside the MHHS. The study from Muthukumar et al. [13] indicated that increasing the heat transfer area by an internal fin leads to the improvement of the local thermal conductivity of the MH bed. Keshari & Maiya [12] employed the internal copper pin fin for $LaNi_5$ MHHS. The pin fin was attached to each other at the centre to the centre and side-by-side. Their study proved that larger fin diameters and higher fin numbers increased heat transfer surface areas, resulting in a higher heat transfer efficiency. Krishna et al. [14] introduced the new fin efficiency concept based on the reverse engineering technique to optimise the MHHS. The number of fins and fin shape were considered for the study purpose. Appropriate selection of the fin's number significantly affects the heat transfer, while the precisely radial tapering had an insignificant impact on the heat transfer performance. The fin thickness of 3 mm was preferred for the use of precisely radial tapering [15]. Some studies also combine internal fin heat exchangers with internal cooling tubes to increase the heat transfer performance and decrease the weight of the overall MHHS, as the main problem of using internal fins only is a higher weight of the overall MHHS. The multiple internal cooling tubes were combined with the fins and placed inside the MHHS [16,17]. The results from these studies proved that the fin number was the key parameter that positively affected the hydrogen absorption rate, compared to fin radius and fin thickness. Bai et al. [18] employed the tree-shaped fins incorporating the central cooling tube for the MHHS. This study indicated that the absorption duration was reduced by 20.7 %, compared to the case with radial fins. This complex fin's structure was the key parameter to increase the heat transfer efficiency. A higher length ratio of these fins increased the heat transfer performance. However, the study from Ayub et al. [19] stated that when using the annular truncated hollow conical fins with a central cooling tube, fin parameters significantly affected the MHHS performance. These fin parameters included fin angle, fin radius, number of fins, fin spacing, and fin thickness. Singh et al. [20] combined circular fins with a U-shape tube heat exchanger for MHHS. This study reported that the overall storage performance could improve when increasing the fin number as well as reducing the fin thickness at the same time. The study by Bai et al. [21] combined both the inner and outer fins and placed them inside the MHHS with a cooling jacket. The uniformity of the temperature distribution in the MH bed was improved when increasing the fin number with the constant fin volume.

Some studies also combined internal fins with helical coil/spiral heat exchangers. Due to the structure of the helical coil heat exchanger, the annular/circular fins could be applied only. The hydrogen absorption duration from this combination was two times less than the case with helical coil heat exchanger only [22,23]. Mellouli et al. [24] proved that the absorption time was decreased by 66 % with the use of a spiral-coil tube and circular fins, compared to the case with the spiral-coil tube only. Krishna et al. [25] proposed a new heat exchanger design, namely a flat coil tube heat exchanger. A spiral fin was integrated with a flat coil tube. This integration obtained 35.3 % and 16.7 % of the hydrogen absorption time when compared to the case with a helical coil tube and double helical coil tubes, respectively. Shrivastav et al. [26] combined the copper fin with phase change material to improve the hydrogen absorption/desorption rate. The copper fin was integrated into both MH and phase change material. This study proved that the hydrogen absorption rate significantly improved by at least 86.5 % when using at least 10 fins, compared to the case without fins. Considering the performance between helical coil and straight tube, the helical coil/spiral coil heat exchanger with the heat transfer fluid (HTF) generally obtains better heat transfer performance compared to the straight tube heat exchanger. This is because the secondary circulation of the coil structure provides more heat transfer surface areas. However, the drawback of the coil heat exchanger is the pressure drop. The amount of pressure loss from the coil tube is higher than the straight tube due to the curvature ratio of itself. The study by Guan et al. [27] stated that a coil tube caused pressure losses by 11–17 % compared to a straight tube. For heat exchanger applications, a small amount of pressure drop is required for the fluid's movement inside the heat exchangers. However, a large amount of pressure drop can negatively affect the system's efficiency and can cause system failure. The heat exchange efficiency and pressure drop should be balanced to maintain the overall performance of the heat exchanger [28].

From the above mention, it can be summarised that the combination of the fin heat exchanger and other heat exchangers, which contain the HTF, significantly improves the heat transfer performance. However, the complex coil's structure significantly causes the pressure drop along the system. Furthermore, most studies only consider the improvement of heat transfer and hydrogen absorption/desorption based on the combination of fins and HTF tubes. The effect of the combination of these heat exchangers on the complete absorption-desorption cycle is still missing. Considering both processes, hydrogen absorption and desorption are one of the main parameters for the design of highly efficient MHHS [29]. As the hydrogen desorption durations are usually larger than the hydrogen absorption durations. This is because of the difference in initial pressure for each process and the reaction-rate hysteresis [30]. Therefore, the duration of a complete hydrogen absorption-desorption cycle is significant for optimising the performance, safety, and cost-effectiveness of the storage systems [31]. Moreover, the comparison of the MH volumes with the HTF tube between with and without additional fins has still not been considered. As the overall volumetric and gravimetric of the MHHS should be prioritised, especially for mobile applications [32]. For the fin design, the fin number and fin length are the key parameters that positively affect the heat transfer performance due to increasing in heat transfer surface area [33,34]. However, there are some limitations to increase these parameters, as the large number of fins or the longer length can suppress convective flows and limit the heat transfer enhancement level [1]. From the literature, the Y-shaped fin obtains better heat transfer performance compared to other conventional fins. However, when considering the MHHS without a cooling jacket, the heat transfer rate of the MH bed around the outer wall of the MHHS is lower than in other areas. This is because the MH bed around this area is far away from the HTF and fin branches. The complex fin's structure is also one of the key parameters that affect the heat transfer enhancement, as the well-arrangement of the fin mass distribution to the MH bed leads to a more uniform temperature distribution and less thermal resistance of the MH bed [18]. In contrast, there are some limitations in the reality to manufacture the complex fin's structure by using conventional manufacturing techniques. The additive manufacturing is required instead [35].

Therefore, the objective of this study is to further enhance the MHHS performance by considering the heat transfer improvement with the use of a fin heat exchanger, which is incorporated with the HTF tube. To achieve this, the simple straight tube of the HTF is used instead of other complex heat exchangers to maintain the pressure level. The effect of pressure losses due to the complex HTF tube's structure is analysed and compared with the simple straight tube. The novel triple-branched fin is first designed to fulfil the requirement of heat transfer efficiency instead of using other complex HTF tube designs by considering an increase in heat transfer surface area corresponding to the appropriate arrangement of fin mass distribution to the MH bed. This design is developed from the conventional Y-shaped fin to further enhance the Y-shaped fin performance under the consideration of the complexity of the fin structure. This new fin structure is also designed to meet the requirements of conventional manufacturing techniques by considering not too much complexity of fin structure. Furthermore, based on the literature, the fin parameters also have a greater influence on the heat transfer performance. Consequently, the effect on various fin parameters is also considered to further enhance the triple-branched fin performance by considering the fin/MH volume. The expectation of this study is to improve hydrogen kinetic reaction and heat transfer performance, especially around the middle area between the Y-shaped fin and the top area, which is close to the outer MHHS wall. To investigate the triple-branched fin performance, several fin designs are provided to compare the performance of these fins with the novel fin design. The average bed temperature of the MHHS as well as hydrogen concentration in the hydrogen absorption/desorption process, are investigated to verify this hypothesis. Moreover, the duration of one complete hydrogen absorption-desorption cycle based on these new designs is estimated in this study. The parametric study based on the operating conditions of the HTF and material of the fin/HTF tube is also considered to investigate the triple-branched fin performance on the heat transfer efficiency as well as the hydrogen kinetic reaction for both processes.

2. System description

The MHHS performance is analysed under the fin geometric study as well as the parametric study. The effect of four different fin designs on the average bed temperature of the MHHS and the hydrogen concentration are compared in this study. The best fin performance is then selected for further improvement under the geometric study and parametric study. The MHHS contains internal 8 fins, which connect to the internal straight tube for the HTF. The angle between each fin is 45°. The height and outer diameter of the MHHS are 80 mm and 50 mm, respectively [36,37]. The HTF tube's diameter is fixed at 8 mm [18]. Both the fin and HTF tube are made of copper. The same dimensions and materials are applied for all cases. For the parametric study, the effect of initial HTF temperatures, heat transfer coefficients between the HTF and MH bed, as well as materials of fin and HTF tube are considered in this section.

2.1. Comparisons between the heat exchangers

The schematic diagram of the MHHS with heat exchanger tube and fins designs is presented in Fig. 1. From Fig. 1a, the inlet and outlet for the hydrogen are at the top of the MHHS, while the HTF is released from the bottom surface of the HTF tube. Figs. 1b to e represent the fin characteristics from four fin designs, including the quadrilateral fin, which is considered as the original fin design or case A (Fig. 1b), Y-shaped fin design I as case B (Fig. 1c), Y-shaped fin design II as case C (Fig. 1d), and triple-branched fin design as case D (Fig. 1e). Fin characteristics and dimensions from these four cases are provided in Fig. 2 and Table 1, respectively. The fin height (H) and width (W) are 18 mm and 1 mm [18], which are constant for all cases. Due to the simple design from case A, there are only fin height and width. However, the other specific parameters of the other three models are various depending on the fin characteristics. L is the length of the Y-shaped fin from the left branch to the right branch, α_y is the angle of the Y-shaped fin section, and α_b is the angle of the middle branch fin from the triple-branched fin section. Other specific parameters are included H_1, L_1, W_1, W_2, and α_1. The MH volume from case A is 140.2 cm^3, while the fin volume from this case is 12.9 cm^3. It should be noted that the reduction of the MH volume

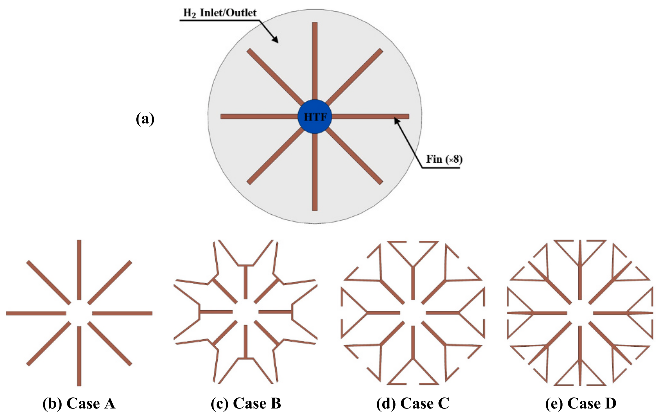

Fig. 1. Storage tanks and fin designs; (a) schematic diagram of MHSS with heat exchanger tube incorporating fins, (b) quadrilateral fin (case A), (c) Y-shaped fin design I (case B), (d) Y-shaped fin design II (case C), and (e) triple-branched fin design (case D).

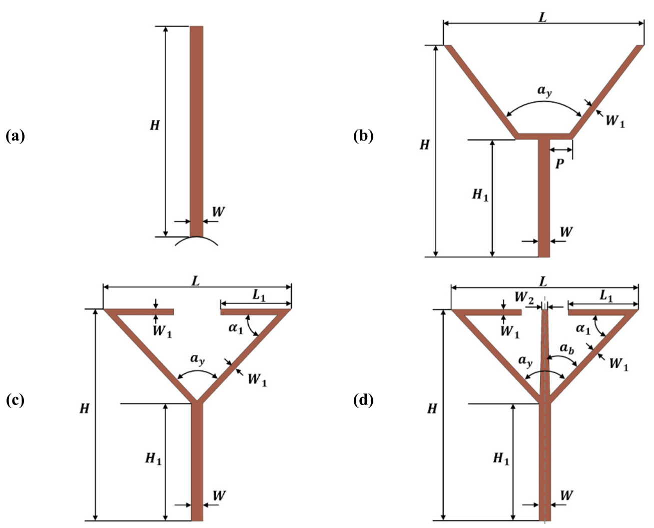

Fig. 2. Characteristics of storage tanks with fin designs; (a) original fin design (case A), (b) Y-shaped fin design I (case B), (c) Y-shaped fin design II (case C), and (d) triple-branched fin design (case D).

from other cases is between 1 and 5 %, compared to case A as the base case. Among these four designs, the best design, that obtains the best heat transfer and hydrogen kinetic reaction performances, is selected to further enhance the fin performance under the fin geometry section.

2.2. Geometric study of triple-branched fin design

From our present study, the new fin design from case D (triple-branched fin) obtains the best performance to enhance the heat transfer efficiency and hydrogen kinetic reaction. The results for four different fin designs can be found in the result and discussion section under “4.2 Performance comparison between different fin designs” Therefore, the fin design case D is selected for further enhancement under the fin parameters. Table 2 provides the fin dimensions with various specific parameters from case D. These include 15 cases, which are from case D and case D-1 to case D-14. The main parameters include fin height, fin angle, fin width, and fin thickness. To study the effect of these parameters, the constant value of each specific parameter from case D is then increased and decreased for comparison purposes. To consider the overall volumetric and gravimetric of the MHHS, the variation of each fin parameter is selected by considering the reduction of the MH volume. The maximum reduction of the MH volume from each parameter is fixed at 1 %. Based on this constraint, the overall MH volume from case D to case D-14 is reduced by less than 5 %. By considering the selected parameters and heat transfer efficiency, the best fin performance is selected for further investigation under the parametric study. The results of the comparison between four different fin designs (case A to case D) are provided under the results and discussion section.

2.3. Parametric study for operating conditions

A parametric study is performed only for the MHHS with the best fin design among case D to case D-14. The parametric study includes the operating conditions of the HTF as well as materials of the fin and HTF tube. Under this section, the initial HTF temperature at 573 K and heat transfer coefficient between the HTF and MH at 500 W m^{-2} K^{-1}, are set as the base values for both absorption and desorption. For all cases, copper is used as the fin and HTF tube materials. Various operating conditions of the HTF are presented in Table 3. These include the HTF temperature from 423 K to 573 K for the absorption and from 573 K to 723 K for the desorption. The heat transfer coefficient between the HTF and MH varies from 250 W m^{-2} K^{-1} to 1000 W m^{-2} K^{-1}. Under fin and HTF tube material, four different materials are selected to compare the performance of heat transfer during hydrogen absorption and desorption. These materials include aluminum, copper, nickel, and steel. Table 4 presents thermos-physical properties of these materials.

3. Mathematical model

All related equations for the numerical simulation are provided in this section. The related equations include the governing equations for both absorption and desorption processes as well as the governing equations for the HTF and fins.

The following assumptions are applied to simply the solution of both hydrogen reactions;

- Thermos-physical properties of hydrogen and metal hydride are constant during both processes [38].
- There is no radiation heat transfer in the MHHS [39].
- Local thermal equilibrium conditions are applied because hydrogen is considered as an ideal gas [40,41].
- The pressure gradient effect of hydrogen injection is negligible [42]. This is because of the following discussion;

$$N = \frac{\lambda_e M L_{gas}^2 \mu}{P_{aeq} \frac{\Delta H^2}{RT^2} \rho_g K L_{heat}^2} \tag{1}$$

where L_{gas} is the tank radius and L_{heat} is the axial height of the tank.

Table 1
Characteristic of the MHSS with four different fin designs; the original fin design (case A), Y-shaped fin design I (case B), Y-shaped fin design I (case C), and triple-branched fin design (case D).

Case no.	H (mm)	W (mm)	L (mm)	P (mm)	α_y (°)	α_b (°)	α_1 (°)	H_1 (mm)	L_1 (mm)	W_1 (mm)	W_2 (mm)
A	18.0	1.0	–	–	–	–	–	–	–	–	–
B	18.0	1.0	17.0	1.9	75	–	–	10.0	–	0.4	–
C	18.0	1.0	16.0	–	86	–	47	10.0	6.0	0.4	–
D	18.0	1.0	16.0	–	86	43	47	10.0	6.0	0.4	0.5

Table 2
Characteristic of fin geometry and selected parameters for case D.

Case No.	H (mm)	W (mm)	L (mm)	α_y (°)	α_b (°)	α_1 (°)	W_1 (mm)	W_2 (mm)	L_1 (mm)	H_1 (mm)
D	18.0	1.0	16.0	86	43	47	0.5	0.5	6.0	10.0
D-1	18.0	1.0	16.0	86	43	47	0.5	0.3	6.0	10.0
D-2	18.0	1.0	16.0	86	43	47	0.5	0.7	6.0	10.0
D-3	18.0	1.0	16.0	86	43	47	0.5	0.7	5.0	10.0
D-4	18.0	1.0	16.0	86	43	47	0.5	0.7	7.0	10.0
D-5	18.0	1.0	16.0	86	43	37	0.5	0.7	7.0	10.0
D-6	18.0	1.0	16.0	86	43	57	0.5	0.7	7.0	10.0
D-7	18.0	1.0	16.0	86	43	49	0.5	0.7	7.0	12.0
D-8	18.0	1.0	16.0	80	40	60	0.5	0.7	7.0	9.0
D-9	18.0	1.0	16.0	74	37	63	0.5	0.7	7.0	8.0
D-10	18.0	1.0	16.0	69	34	66	0.5	0.7	7.0	7.0
D-11	18.0	1.0	15.0	65	32	62	0.5	0.7	7.0	7.0
D-12	18.0	1.0	17.0	72	36	64	0.5	0.7	7.0	7.0
D-13	18.0	1.0	17.0	72	36	64	0.3	0.7	7.0	7.0
D-14	18.0	1.0	17.0	72	36	64	0.7	0.7	7.0	7.0

The highlighted sections refer to the change for each selected parameter.

Table 3
Operating HTF values.

Parameters	Base value	Selected value
HTF inlet temperature for absorption (K)	573	423, 473, 523
HTF inlet temperature for desorption (K)	573	623, 673, 723
Heat transfer coefficient between HTF and MH for absorption and desorption (W m^{-2} K^{-1})	500	250, 750, 1000

Table 4
Thermo-physical properties of different materials for fin and HTF tube.

Material	Density (kg m^{-3})	Specific heat (J kg^{-1} K^{-1})	Thermal conductivity (W m^{-1} K^{-1})
Aluminum	2719	871.0	202.4
Copper	8978	381.0	387.6
Nickel	8900	460.6	91.7
Steel	8030	502.5	16.3

When N is less than 0.01, the flow of hydrogen inside the MHHS can be omitted in the simulation without a significant error [43]. In all simulations from this study, N is significantly less than 0.01. Therefore, the pressure gradient effect is not considered. To simplify the model, the HTF is not simulated in this study. The convection boundary condition is applied on the tube wall to consider the effect of HTF in the tube, which is based on the calculation from the Reynolds number and Prandtl number [44,45].

- There is no heat transfer between the MHHS and the ambient as the wall of the MHHS is well insulated [46].

This study uses Mg_2Ni as the MH material as it provides a faster hydrogen kinetic reaction than other metal hydrides [47]. Moreover, the main advantages of this material are a high hydrogen storage capacity, lightweight, and excellent heat resistivity [48,49].

3.1. Governing equations

3.1.1. Absorption and desorption process

The energy equation for this present study is based on the thermal equilibrium between hydrogen and Mg_2Ni hydride, which is expressed as [50]:

$$\frac{\partial\left(\left(\rho C_p\right)_{e,MH}T\right)}{\partial t} = \nabla\cdot\left(\lambda_{e,MH}\nabla T\right) + \frac{\rho_{MH}c(1-\varepsilon)\Delta H}{M_{H_2}}\frac{\partial X}{\partial t} \tag{2}$$

where the effective heat capacity and conductivity are given as:

$$\left(\rho C_p\right)_{e,MH} = \varepsilon_{MH}\times\rho_{H_2}\times C_{p,H_2} + (1-\varepsilon_{MH})\times\rho_{MH}\times C_{p,MH} \tag{3}$$

$$\lambda = \varepsilon_{MH}\times k_{H_2} + (1-\varepsilon_{MH})\times\lambda_{MH}. \tag{4}$$

The hydrogenation reaction of Mg_2Ni bed (ΔH) is determined as:

$$Mg_2Ni + 2H_2 \leftrightarrow Mg_2NiH_4 + \Delta H. \tag{5}$$

The amount of hydrogen absorption/desorption on metal surface (in wt%) is denoted as X. This can be obtained based on the kinetic reaction. For hydrogen absorption, the kinetic equation during this process is calculated based on the following equation [51]:

$$\frac{\partial X}{\partial t} = C_{abs}exp\left(\frac{-E_{abs}}{RT}\right)\left(\frac{P_{H_2}-P_{abs,eq}}{P_{abs,eq}}\right)(X_{max}-X). \tag{6}$$

For hydrogen desorption, the kinetic equation during this process is calculated based on the following equation [45]:

$$\frac{\partial X}{\partial t} = C_{des}exp\left(\frac{-E_{des}}{RT}\right)\left(\frac{P_{H_2}-P_{des,eq}}{P_{des,eq}}\right)(1-X) \tag{7}$$

where C_{abs} and C_{des} are the reaction rate constant for absorption and desorption, while E_{abs} and E_{des} refer to activation energy for absorption and desorption, respectively. The equilibrium pressure inside the MHHS for the absorption process ($P_{abs,eq}$) and desorption process ($P_{des,eq}$) are determined by using Van't Hoff equations. Eq. (8) refers to the equilibrium pressure during the absorption [50], while Eq. (9) is for the equilibrium pressure during the desorption [45]:

$$ln\frac{P_{abs,eq}}{P_{ref}} = -\frac{7618}{T} + 14.534, \tag{8}$$

$$ln\frac{P_{des,eq}}{P_{ref}} = -\frac{7614}{T} + 14.049, \tag{9}$$

where P_{ref} denotes as the reference pressure as 0.1 MPa. Thermo-physical properties of hydrogen and Mg_2Ni are provided in Table 5.

3.1.2. Heat transfer fluid and fins

The continuity equation for the HTF is as the following equation:

$$\nabla\vec{v}_f = 0, \frac{\partial T_f}{\partial t} = 0. \tag{10}$$

Table 5
Thermo-physical parameters of hydrogen and metal hydride in model equations [39,45,50,52].

Parameters	Symbols	Values
Molecular weight of MH	M_{MH}	0.1073 kg mol^{-1}
Hydride specific heat	$C_{p,MH}$	1414 J kg^{-1} K^{-1}
Density of MH	ρ_{MH}	3200 kg m^{-3}
Density of saturated MH	$\rho_{ss,MH}$	3319.32 kg m^{-3}
Reaction enthalpy	ΔH	−63,336 J mol^{-1}
Reaction entropy	ΔS	−120.84 J mol^{-1} K^{-1}
Reaction rate constant for absorption	C_{abs}	175.07 s^{-1}
Reaction rate constant for desorption	C_{des}	2079 s^{-1}
Activation energy for absorption	E_{abs}	49,674 J mol^{-1}
Activation energy for desorption	E_{des}	63,540 J mol^{-1}
Porosity	ε	0.5
Effective thermal conductivity of MH	$\lambda_{e,MH}$	0.674 W m^{-1} K^{-1}
Maximum concentration of hydrogen in the MH	X_{max}	1.0
Initial concentration of hydrogen in the MH	X_0	0.043
Permeability	K	1×10^{-8} m^2
Density of hydrogen	ρ_{H2}	0.32 kg m^{-3}
Thermal conductivity of hydrogen	λ_{H2}	0.167 W m^{-1} K^{-1}
Specific heat of hydrogen	$C_{p,H2}$	14,890 J kg^{-1} K^{-1}
Dynamic viscosity of hydrogen	μ_{H2}	8.41×10^{-6} Pa s
Molecular weight of hydrogen	M_{H2}	0.002 kg mol^{-1}

The heat transfer coefficient (h_f) between the HTF and MH bed is calculated based on the following equation:

$$h_f = \frac{\lambda_f}{d} Nu_f. \tag{11}$$

In this study, various values of the heat transfer coefficient (h_f) between the HTF and MH bed are selected and applied to analyse the effect of this parameter on the heat transfer efficiency of the heat exchanger. This can be found under the parametric study section. The Nusselt number (Nu_f) for the internal straight tube, which is used for the air as the HTF, can be calculated based on turbulent flow (Eq. (12)) [45,53]:

$$Nu_f = 0.012\left(Re_f^{0.87} - 280\right)Pr_f^{0.4}\left[1 + (d/L_{HTF})^{2/3}\right](Pr_f/Pr_{MH})^{0.11} \tag{12}$$

where Re_f is the Reynolds number and Pr_f is Prandtl number. These two parameters can be obtained based on the following equation:

$$Re_f = \frac{\rho_f d v_f}{\mu_f}, Pr_f = \frac{\mu_f C_{pf}}{\lambda_f} \tag{13}$$

For copper fins, the energy equation for the heat conduction is expressed as:

$$\left(\rho C_p\right)_{fin}\frac{\partial T}{\partial t} = \lambda_{fin}\nabla^2 T \tag{14}$$

where $\left(\rho C_p\right)_{fin}$ is the heat capacity of copper fins.

It should be noted that conditions from above mentioned are applied for all simulations, except the effect of pressure losses due to the heat exchanger structures. Under the study of pressure variation along the heat exchanger tubes, the turbulent HTF flow is selected under the realizable k-ε turbulence model with a velocity at 76.86 m s^{-1} and a Reynolds number of 9000. Air is selected as the HTF for this study. The selected turbulence model was validated against the experimental study in our previous study [54]. The governing equations under this section can be found in our previous study [36].

3.2. Initial and boundary conditions

Refer to our previous studies [36,54], the initial conditions of the MHHS for the hydrogen absorption process are 573 K of the temperature ($T_{MH,abs} = T_{0,abs}$) and 1.8 MPa of the loading pressure ($P_{0,abs}$). For the hydrogen desorption process, the initial conditions of the MHHS are the ultimate temperature of the absorption ($T_{MH,des} = T_{ultimate,abs} = T_{0,des}$) and 0.1 MPa of the hydrogen pressure ($P_{0,des} = P_a$). Air is selected at the HTF. The HTF temperature from the internal straight tube heat exchanger is fixed as 573 K for both absorption and desorption ($T_{HTF,abs} = T_{HTF,des}$). The heat transfer coefficient (h_f) between the HTF and the MH bed is constant at 500 W m^{-2} K^{-1} for both processes. It should be noted that the same conditions are applied for all simulation cases under the fin designs and optimisation. However, the values of HTF temperature and h_f are varied under the parametric study.

Adiabatic wall of the storage:

$$\frac{\partial T_{MH}}{\partial \vec{n}} = 0 \tag{15}$$

Wall of the heat exchanger tube:

$$\lambda_e \frac{\partial T_{MH}}{\partial \vec{n}} = h_f\left(T_f - T_{MH}\right) \tag{16}$$

3.3. Numerical schemes, grid independence, and model validation

3.3.1. Numerical schemes and grid independence

A typical 1/4 unit of the whole storage container is used for all numerical simulations due to the symmetric structure of the MHHS, allowing a reduction of computation time. The commercial software, namely ANSYS Fluent 2021 R2 is used for all computational simulations. The user-defined functions (UDFs) are applied for the energy source terms to propose the kinetic reactions during hydrogen absorption/desorption. The SIMPLE algorithm is used to tackle the pressure-velocity coupling. The second-order upwind scheme is selected for pressure, momentum, and energy equations with the convergence criteria as 10^{-6}.

3.3.2. Grid independence and model validation

The model validations for the MHSS during the absorption and desorption processes under the use of Mg_2Ni alloy are provided in our previous studies [37]. These validations were performed based on the comparison between our previous study [37] and the studies from Muthukumar et al. [47], Wu et al. [45], and Wu et al. [50]. Grid refinement tests were performed for different grid sizes for the hydrogen absorption process to achieve accurate simulation results. Due to the same MHHS and heat exchangers, case B is selected. The same meshing techniques are then applied to the other cases. From Table 6, it is obvious that the average bed temperature and absorption time become stable and have minor changes at 436,416 element numbers for case B. Based on these elements, the average bed temperature is 620.19 K, with the absorption time at 4297 s. Therefore, these element numbers are chosen for further studies.

4. Results and discussion

The effect of heat exchanger types on pressure variation along the inlet throughout the outlet is analysed in this section. The investigation of this effect is based on the use of HTF and pressure loss due to the heat exchanger's structure. The best heat exchanger performance is then selected to integrate with the fin heat exchanger to further heat transfer enhancement. Furthermore, the simulated results of the MHHS based on various fin designs for hydrogen absorption/desorption are then provided. The average bed temperature of the MHHS and the hydrogen concentration based on these fin designs are also included in this section

Table 6
Effect of different grid numbers on the hydrogen absorption time and average bed temperature for case B.

No.	Number of elements	Average bed temperature (K)	Absorption time (s)
1	172,837	620.77	4361
2	221,973	620.57	4317
3	436,416	620.19	4297
4	622,554	619.29	4292

for comparison purposes. The best fin performance, which obtains the best heat transfer efficiency and hydrogen kinetic reaction rate, is selected to further enhance the fin efficiency under various selected parameters. Finally, the best fin geometry with appropriately selected parameters is then chosen to analyse its performance in the parametric study section.

4.1. Pressure variation along the heat exchangers

The effect of heat exchanger types on the pressure variation from the inlet throughout the outlet is analysed and presented in Fig. 3 under the pressure contour. The comparison is provided under the same boundary conditions, which include the inlet flow velocity as 76.86 m $s^{-1}$and air as the HTF. In this section, the selected material of the HTF tube is stainless steel. The heat exchanger types in this study include the straight tube heat exchanger (STHE), helical coil heat exchanger (HCHE), semi-cylindrical coil heat exchanger (SCHE), and semi-cylindrical coil heat exchanger with central return tube (SCHE-CR). The heat transfer performance based on these heat exchangers was analysed in our previous study [36,37,54,55]. The HCHE and SCHE (×2) are designed under the constant volume at 15.34 cm^3, while the SCHE-CR (×2) has the volume at 17.12 cm^3. The volume of the STHE is 1.01 cm^3. The tube diameter of all heat exchangers is fixed at 4 mm for comparison purposes. Under the same fluid velocity at the inlet, the pressure contour from Fig. 3 indicates that the cases with coil tube structure have higher pressures, especially at the inlet. The inlet pressure from these cases is over 147,646 Pa. However, the pressure decreases along the coil tube from the inlet throughout the outlet, which has a pressure of 98,738 Pa. This is due to the effect of the curvature ratio of the coil tube, which requires more power to inject the HTF from the inlet and circulate throughout the heat exchanger. In contrast, the pressure difference from the STHE is very small. The inlet pressure is only around 109,218 Pa, while the outlet pressure is around 98,738 Pa.

More analysis regarding the effect of heat exchanger types is provided in Fig. 4 and Fig. 5. This includes the range of skin friction coefficient from each design along the heat exchanger tube (Fig. 4a) and the effect of heat exchanger type on pressure losses from the inlet throughout the outlet (Fig. 4b). It should be noted that the percentage is calculated based on the maximum pressure between the inlet and the outlet of each heat exchanger. Fig. 5 refers to the heat transfer surface area from each heat exchanger type (Fig. 5a) and the hydrogen absorption/desorption duration from various heat exchangers (Fig. 5b). From Fig. 4a, the minimum skin friction coefficients from all heat exchanger types are less than 10. However, the maximum skin friction coefficients at the inlet of these heat exchangers are different. The maximum values from STHE, HCHE, SCHE, and SCHE-CR are 28, 31.51, 35.64, and 43.76, respectively. The skin friction coefficient refers to the ratio of the wall shear stress and the reference dynamic pressure. The equation of skin friction coefficient is as follows,

$$C_f = \frac{\tau_\omega}{\frac{1}{2}\rho U_\infty^2}, \tag{17}$$

where C_f is the skin friction coefficient, τ_ω is the wall shear stress, ρ is fluid density, and U is the free-stream velocity (at the inlet). Based on the boundary conditions from this study, the density of fluid and inlet velocity are constant for all designs. However, the results from Fig. 4a are different. This means that the wall shear stress is only the one parameter that affects the difference in the skin friction coefficients between different designs. In general, the wall shear stress depends on the fluid velocity when moving from the tube wall toward the centre of the tube. Due to the complex design of all coil cases, it generates a turbulent flow inside the tube. The results of the turbulent level of fluid flow inside the tube can be found in our previous study [36]. Therefore, a higher velocity magnitude from these cases obtains a higher wall shear stress, which leads to a higher skin friction coefficient. During fluid flowing in the tube, there is a combination of the tangential force at the wall and the viscous shear stress at the wall, which acts in the opposite direction to the direction of fluid motion [56]. A higher pressure at the tube inlet is required when these parameters have higher values [56]. As a result, this phenomenon affects the amount of pressure drop inside the tube. The results from Fig. 4b prove that there are more pressure losses from the coil tube structure compared to the straight tube. There is around 34 % pressure loss between the inlet and outlet from these complex heat exchangers. However, there is only a 3 % pressure loss from the inlet to the outlet from the case with the straight tube. In general, the pressure drop is the result of the friction which is caused by the HTF rubbing against the inner wall of the tube. The HTF will require more power to overcome the friction inside the longer tube, compared to the shorter tube. In other words, a longer tube will obtain a higher pressure drop than a short tube [28]. This is obvious in the results from Fig. 5a, as the STHE has a shorter length with only 10 cm^2 of heat transfer surface area, while the other cases have a longer length due to the coil's effect with the range of 150–172 cm^2 of heat transfer surface area. It should be noted that the difference in the percentage of the pressure loss and heat transfer surface area in coil cases can be because of the difference in the curvature ratio of each coil design. A higher curvature ratio can obtain a higher pressure loss. Considering the effect of heat exchanger types on the one complete cycle of hydrogen absorption-desorption from Fig. 5b, the duration of the one complete cycle from the HCHE, in this case, is 38,646 s. When using the SCHE, this duration is reduced to 25,147 s. However, when using the central return tube as the SCHE-CR, this duration is further reduced to 17,279 s. Therefore, using the coil tube significantly improves the heat transfer rate inside the storage system,

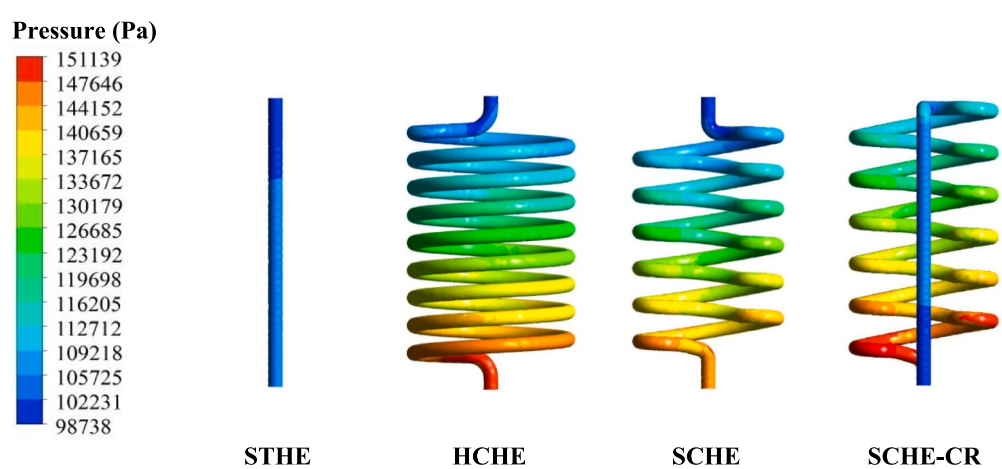

Fig. 3. Pressure variation from various heat exchangers.

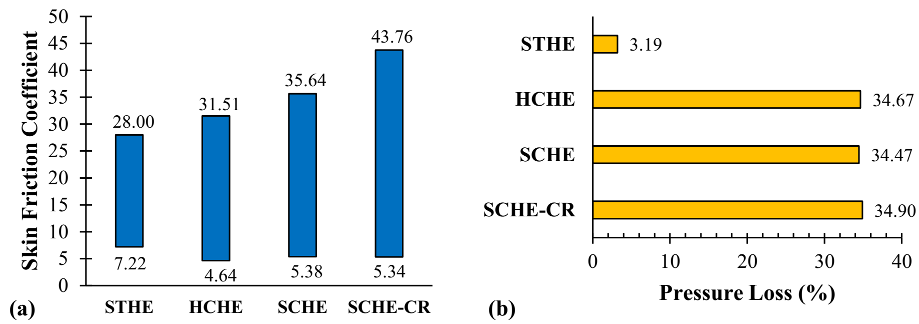

Fig. 4. Skin friction coefficient and pressure losses from various heat exchangers; (a) skin friction coefficient and (b) pressure loss.

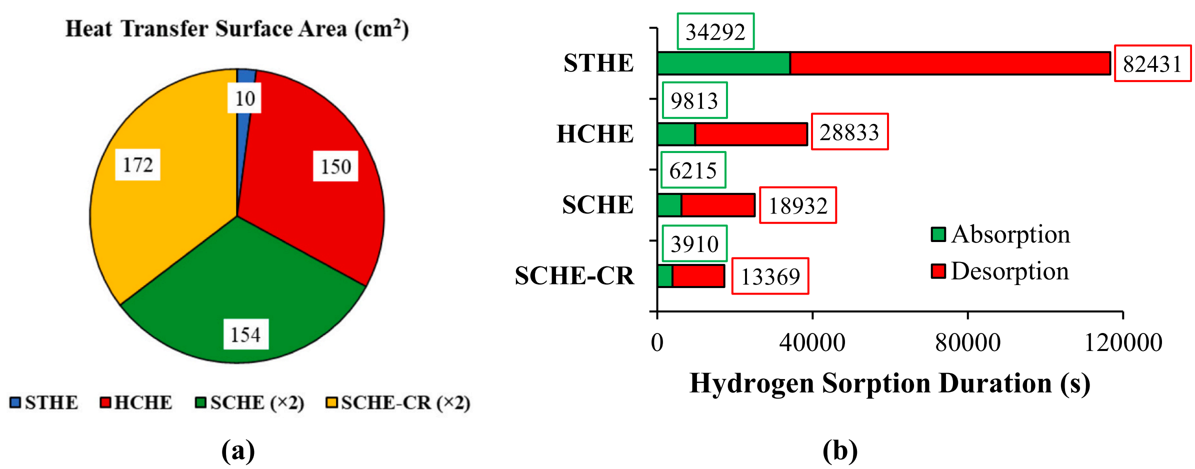

Fig. 5. Heat transfer surface area and hydrogen sorption duration from various heat exchangers; (a) heat transfer surface area and (b) hydrogen absorption/desorption duration.

leading to a reduction in hydrogen absorption/desorption duration. This is because of an increase in the heat transfer surface area of the coil tube from the secondary circulation of itself [50]. The STHE case has less heat transfer surface area leading to less heat transfer efficiency, compared to the coil tube cases. This negatively affects the hydrogen absorption/desorption duration. The final time of this one complete cycle from this case is 116,723 s. From these results, it is obvious that there are 67 %, 78 %, and 85 % reductions in duration for one complete cycle when using HCHE, SCHE, and SCHE-CR instead of STHE. It should be noted that the absorption and desorption from these cases are obtained based on the stainless steel tube of the HTF. Other materials with a high thermal conductivity, such as copper, aluminum, and nickel, can enhance the rate of hydrogen kinetic reaction, resulting in faster hydrogen absorption/desorption. Although the straight tube has less heat transfer efficiency, the straight tube has minor pressure losses compared to the coil tube. As the excessive pressure drops (from inlet to outlet) will significantly result in a negative system's efficiency and excessive energy consumption [28]. The straight tube is then selected for further study by combining itself with the fin heat exchangers. The effect of this combination on the heat transfer efficiency and hydrogen absorption-desorption duration is provided in the next section.

In general, air and water are commonly selected as the HTFs for the MHHS due to their advantages that they offer low cost and less environmental impact, compared to other HTFs. However, due to a high operating temperature range of Mg2Ni, air is selected as the HTF for this study. Furthermore, air also offers better flow characteristics when compared to other liquid metals and molten salt [57]. Considering the effect of pressure loss due to the HTF, the use of air as the HTF significantly causes huge pressure losses, especially when using complex heat exchangers. However, the effect of pressure loss might be insignificant when employing other HTFs with different thermal-physical properties.

4.2. *Comparisons between the fin designs*

The comparison of average bed temperature and hydrogen concentration during the hydrogen absorption under four different fin designs is presented in Fig. 6. Case A refers to the MHHS with a quadrilateral fin, while case B and case C are for the MHHS with Y-shaped fin design I and Y-shaped fin design II. Case D refers to the MHHS with the new fin design, namely the triple-branched fin. For all cases, the MHHS temperature is fixed as 573 K with loading pressure at 1.8 MPa. The HTF temperature is constant at 573 K with the heat transfer coefficient at 500 W m^{-2} K^{-1}. From this figure, there is an interaction between the metal alloy and hydrogen when the hydrogen is initially injected into the MHHS. This leads to a rapid increase in MH bed temperature and slowly increase to reach the maximum point. The MH bed temperature then continually decreases due to the heat transfer effect from the HTF and fins. The generated heat during this stage must be removed from the system to control the desired charging rate during this stage [52]. A faster MH bed temperature reduction causes a faster hydrogen kinetic reaction, resulting in faster hydrogen absorption [52]. The more fin mass distribution to the MH bed leads to the more uniform temperature distribution to the MH bed [18]. The results from Fig. 6 also support this fact. The average MH bed temperature from case A reduces slower than case B, resulting in slower hydrogen absorption from case A, compared to case B. The final time of the absorption process from case A is 4919 s, while it is only 4297 s from case B. Due to more fin mass distribution to the MH bed from case C and case D, the heat is transferred faster than in the first two cases. However, the absorption duration from case D is still shorter than case C due to the effect of the new fin design, which

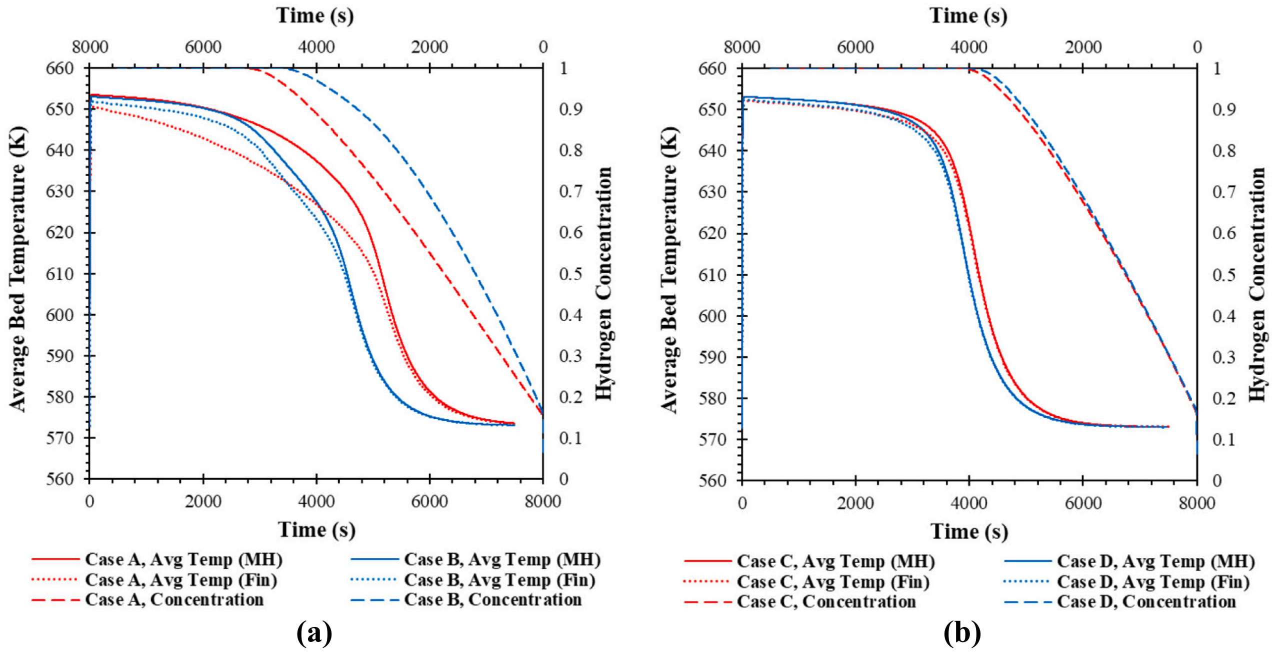

Fig. 6. Average bed temperature and hydrogen concentration from all cases; (a) case A, case B and (b) case C, case D. (The solid line is for average bed temperature, the large dashed line is for hydrogen concentration, and the small dashed line is for average fin temperature).

provides more fin mass distribution. The absorption duration from case C is 3848 s, while it is 3680 s from case D. More discussion regarding the temperature difference is provided in the next section.

For more analysis, temperature contours and hydrogen concentration contours along the MHHS with different fin designs are presented in Fig. 7. The selected times, including 2500 s and 3500 s, after starting the hydrogen absorption, are provided in this figure. From Fig. 7a, the central area from all designs has the lower temperature because it directly connects with the HTF tube, which is located at the central area of the MHHS. The MH, which is close to the fin area, also has a lower temperature. This is due to the metal fin ability, which conducts and transfers the heat between the HTF and MH. At 2500 s, the fin temperature from case A is significantly lower than the fin temperatures from other cases. This is due to the complex fin structure from other cases, which has more fin mass distribution in the MH bed around the outer part of the MHHS. This requires longer times to conduct and transfer the heat between the HTF tube and copper fins. In other words, the heat is then further transferred from the MH beds to the HTF tube via the copper fins [18]. The MH bed temperature from most areas around the outer wall of the MHHS from case A is still higher, compared to other cases. Similarly, most outer areas from case B still have a higher temperature, compared to case C and case D. This is due to the complex fin design. The more fin mass distribution leads to the reduction in heat conduction resistance of the MH bed, resulting in a more uniform MH bed temperature [18]. It is obvious that at the top parts of the Y-shaped fin from case C and D, more uniform temperature distributions occur around these parts. However, due to the complex fin design from case D, which increases more fin areas, especially at the centre of the Y-shaped fin, the outer areas of the MHHS have lower temperatures compared to case C. The significant changes in the temperature variation between these four cases are observed at 3500 s. A high MH bed temperature, especially around the outer areas, is still observed from case A and case B. The MH bed temperature from case D is more uniform and significantly lower than in other cases. It is obvious that increasing the fin areas from the Y-shaped fin (case B) obtains better heat transfer performance inside the MHHS, especially from the tripled-branched fin (case D). In hydrogen absorption, faster heat removal from the system causes a faster hydrogen absorption. In other words, lower MH temperatures mean higher hydrogen concentrations. The hydrogen concentration contours from Fig. 7b can support this fact, as around the HTF and fin areas usually have a higher hydrogen concentration. This is because these areas have lower temperatures, compared to other areas (refer to temperature contours from Fig. 7a). Due to the complex fin structure from case C and case D, the concentration at the outer areas from these cases is always higher than another two cases (case A and case B). The significant difference in hydrogen concentration is observed at 3500 s as case A and case B still have less hydrogen concentration around the outer areas of the MHHS.

Fig. 8 presents the comparison of MH volume/fin volume and its effects on the absorption duration from all cases. From Fig. 8a, there is a 0.9 % reduction of MH volume from case A (base case) to case B, while there are 2.7 % and 5.2 % reductions of MH volume from case A to case C and from case A to case D, respectively. However, considering the absorption duration from all cases from Fig. 8b, (refer to the discussion from Fig. 6), the reductions of absorption duration from case A to case D are 12.6 %, 21.8 %, and 25.2 %, respectively. It is obvious that case D obtains the best performance in terms of heat transfer efficiency and hydrogen absorption, compared to the other cases. Therefore, case D is selected for further investigation to enhance its performance.

4.3. *Geometric study of triple-branched fin design (case D)*

This section provides a comprehensive study of the fin geometry for the triple-branched fin (case D) based on the constant operating conditions. The fin performance based on various fin parameters is investigated under the comparison of MH temperature at selected locations during the hydrogen absorption. These various fin parameters and values are defined into 15 cases (case D, and case D-1 to case D-14). Fig. 9 presents the selected locations to compare the MH temperature based on various fin parameters. It should be noted that these locations are randomly selected to obtain the best comparison for the temperature variation.

4.3.1. *Influence of fin thickness at the middle branch (W_2) and fin width at the top branch (L_1)*

Effects of fin thickness at the middle branch (W_2) and fin width at the

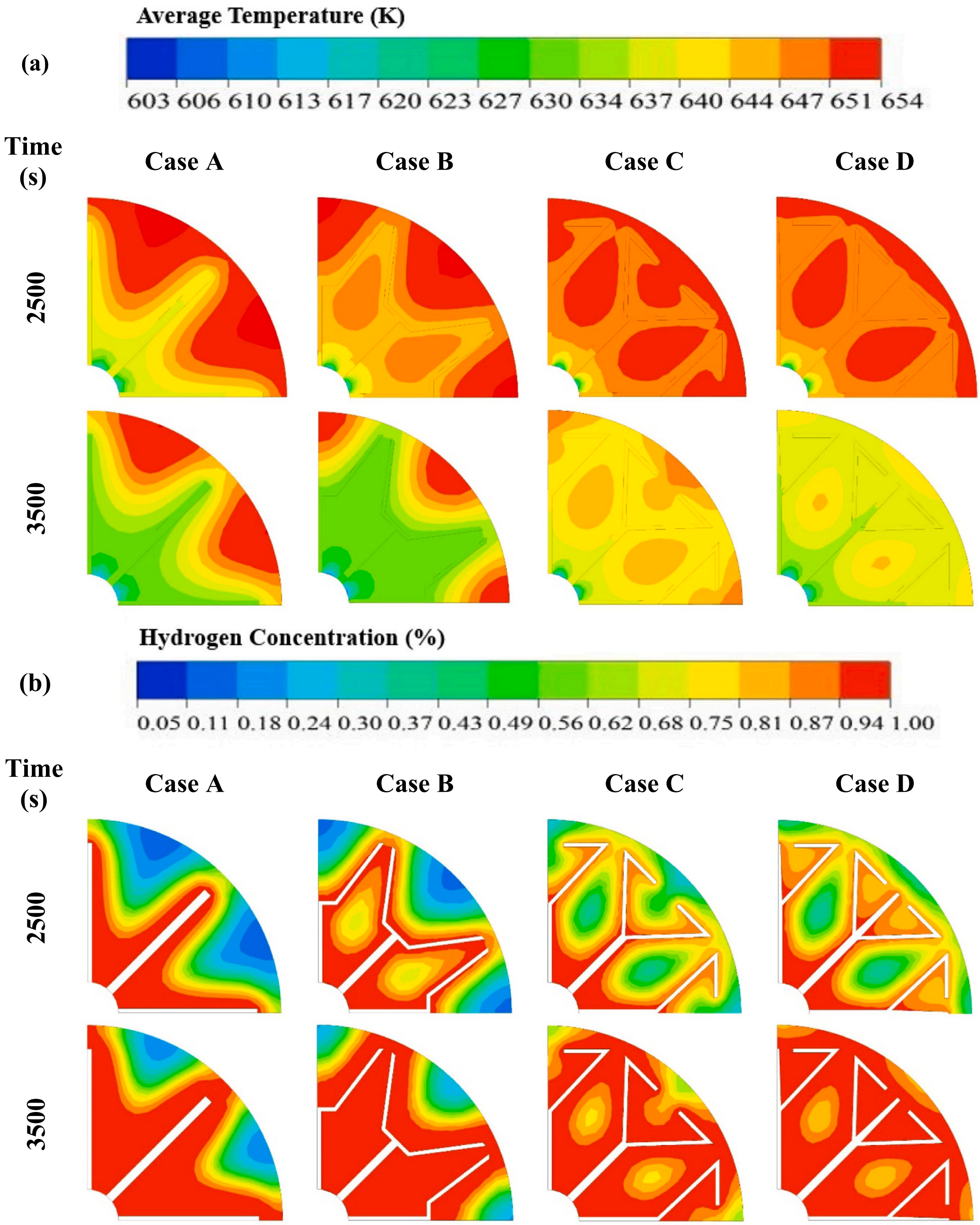

Fig. 7. Average temperature and hydrogen concentration of MH bed and fins at 2500 s and 3500 s after starting hydrogen absorption process in all cases; (a) average temperature and (b) hydrogen concentration.

top branch (L_1) on the temperature at the selected points along the MHHS are presented in Fig. 10. From Fig. 10a, the MH temperature at P1 is reduced when increasing the fin thickness at the middle branch (W_2). The comparison from this parameter is made based on three different fin thicknesses at this branch from case D (0.5 mm thickness), case D-1 (0.3 mm thickness), and case D-2 (0.7 mm thickness). From Fig. 10b, the MH temperature at P1 is also reduced faster when increasing the fin width at the top branch (L_1). The three different values are selected for the comparison, including 6 mm for case D-2, 5 mm for case D-3, and 7 mm for case D-4. From these two parameters, the temperatures from these cases have minor differences due to the minor differences in the fin thickness in this area and fin width at the top branch. One of the main reasons is that the tapering of fin thickness (W_2) is distributed to a larger amount of the MH, compared to the other side [14]. However, the difference in MH volume from these three cases is still less than 1 %.

4.3.2. *Influence of fin angle (α_1), fin height (H_1) and fin width (L) for triple-branched section*

The effects of the fin angle of the top branch (α_1), fin height (H_1) and fin width (L) for the triple-branched section on the temperature variation are presented and compared in Fig. 11 based on the selected points at P2 to P7. Three different values of the fin angle include 47° (case D-4), 37° (case D-5), and 57° (case D-6). From Fig. 11a, it can be seen that the fin angle (α_1) only slightly affects the MH bed temperature at P2.

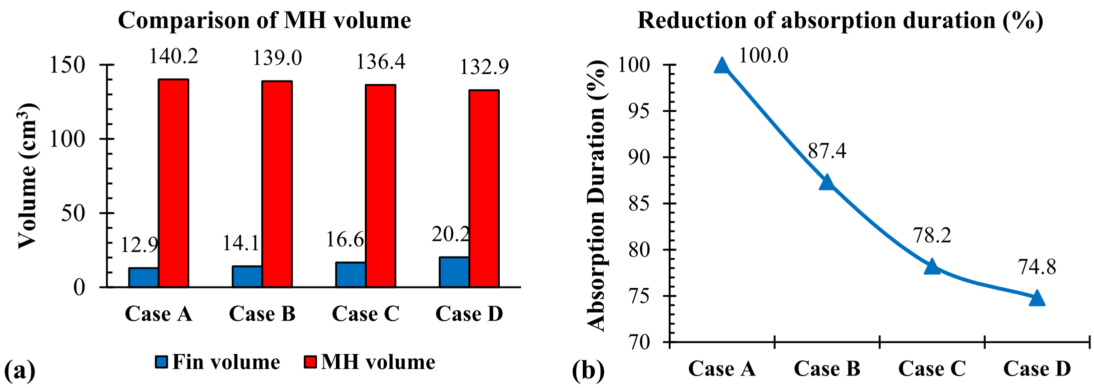

Fig. 8. Comparison of all four cases during the hydrogen absorption. (a) comparison of MH volume and (b) reduction of absorption duration.

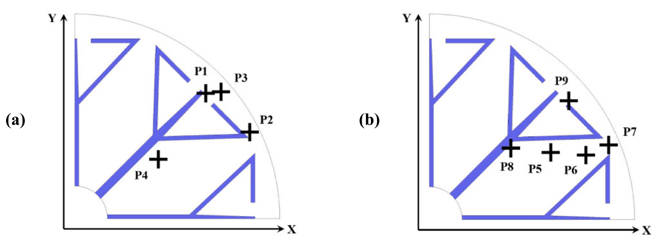

Fig. 9. Selected points for the comparison of storage bed temperature during the hydrogen absorption; (a) at P1 to P4 and (b) at P5 to P9.

However, the greater fin angle at 57° (case D-6) causes a greater MH temperature reduction at P3 from Fig. 11b. The MH temperature at 3500 s in this case is greatly lower than in other cases. The difference in MH temperature between the lowest angle and the highest angle is 6 K. Based on this parameter, there is only a 1 % reduction of MH volume from case D-6, compared to other cases. Therefore, fin angle significantly affects the improvement of heat transfer inside the MHHS, especially around the outer wall of the MHHS. This is due to more fin mass distribution to this area. Considering the fin height, five different values of fin height are selected for this study, including 10 mm (case D-6), 12 mm (case D-7), 9 mm (case D-8), 8 mm (case D-9), and 7 mm (case D-10). From Fig. 11c, d, it is obvious that reducing the fin height (H_1) results in a faster MH temperature reduction. This is because it increases the triple-branched area. The length of the left and right branches from this fin design is increased because of this height. The effect of branching becomes advantageous due to the greater thermal penetration depth into the system [31]. This results in a more uniform temperature distribution along these fin areas. Comparing between the highest fin height and the lowest fin height at 3500 s of absorption time, the MH temperatures at P4 are 5 K in difference, while the MH temperatures at P5 are 9 K in difference. The MH volume from all cases only reduces by around 1 %, comparing between case D-7 and case D-10. Therefore, the fin height for the triple-branched section also greatly affects the heat transfer performance inside the MHHS. Considering the fin width (L) from Fig. 11e, f, the different fin widths for the triple-branched section include 15 mm (case D-11), 16 mm (case D-10), and 17 mm (case D-12). At 3500 s, the MH temperature at both P6 and P7 from the lowest fin width is 637 K, while the MH temperature at these points from the highest fin width is 633 K. The MH temperature from these points indicates that the larger fin width at the triple-branched section positively affects the heat transfer performance. Similar to the fin height, the larger fin width leads to an increase in the overall length at the Y-shaped branch section, resulting in more fin mass distribution to the MH bed. Under this parameter, the difference in MH volume is only less than 0.5 %.

4.3.3. Influence of fin thickness at side branches (W_1)

Fig. 12 demonstrates the MH temperature at P8 (Fig. 12a) and P9 (Fig. 12b) under the influence of fin thickness at the first and third branches (W_1). Three different fin thicknesses are selected in this section. These include 0.3 mm (case D-13), 0.5 mm (case D-12), and 0.7 mm (case D-14). Although fin thickness is not the critical fin parameter, there is an optimal thickness. The thicker fin can reduce the rate of enhancement effect [58]. From Fig. 12, it is obvious that increasing the thickness of the triple-branched fin significantly enhances the heat transfer rate. The MH temperature from a higher fin thickness is usually lower than the lower fin thickness. Increasing the fin thickness leads to an increase in heat transfer surface areas. At 3500 s, the MH temperature at P8 from the thickness of 0.7 mm is 14 K less than the case with 0.3 mm thickness, while it is 15 K less than 0.3 mm thickness at P9. Therefore, the fin thickness of 0.7 mm still positively affects the heat transfer rate. However, the MH volume is reduced by 6 %, comparing between 0.3 mm and 0.7 mm thickness.

Fig. 13 shows the hydrogen concentration contours for the hydrogen absorption process between case D (before enhancement) and case D-14 (after enhancement). In both cases, around the central area has a higher

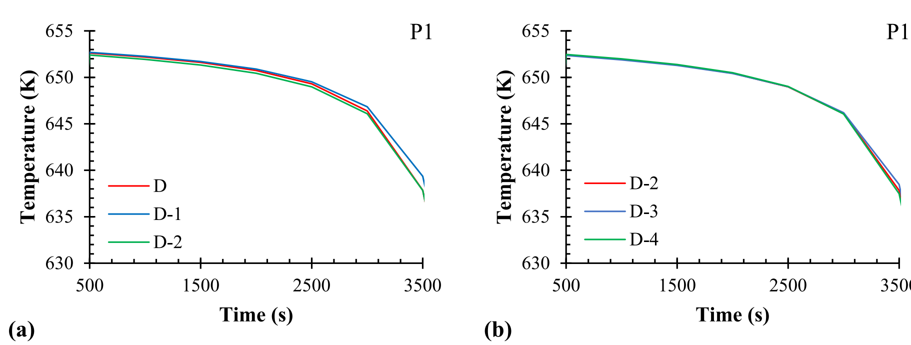

Fig. 10. Temperature at selected point, P1 based on the fin parameters (from case D to case D-4); (a) fin thickness at second branch and (b) fin width at top branch.

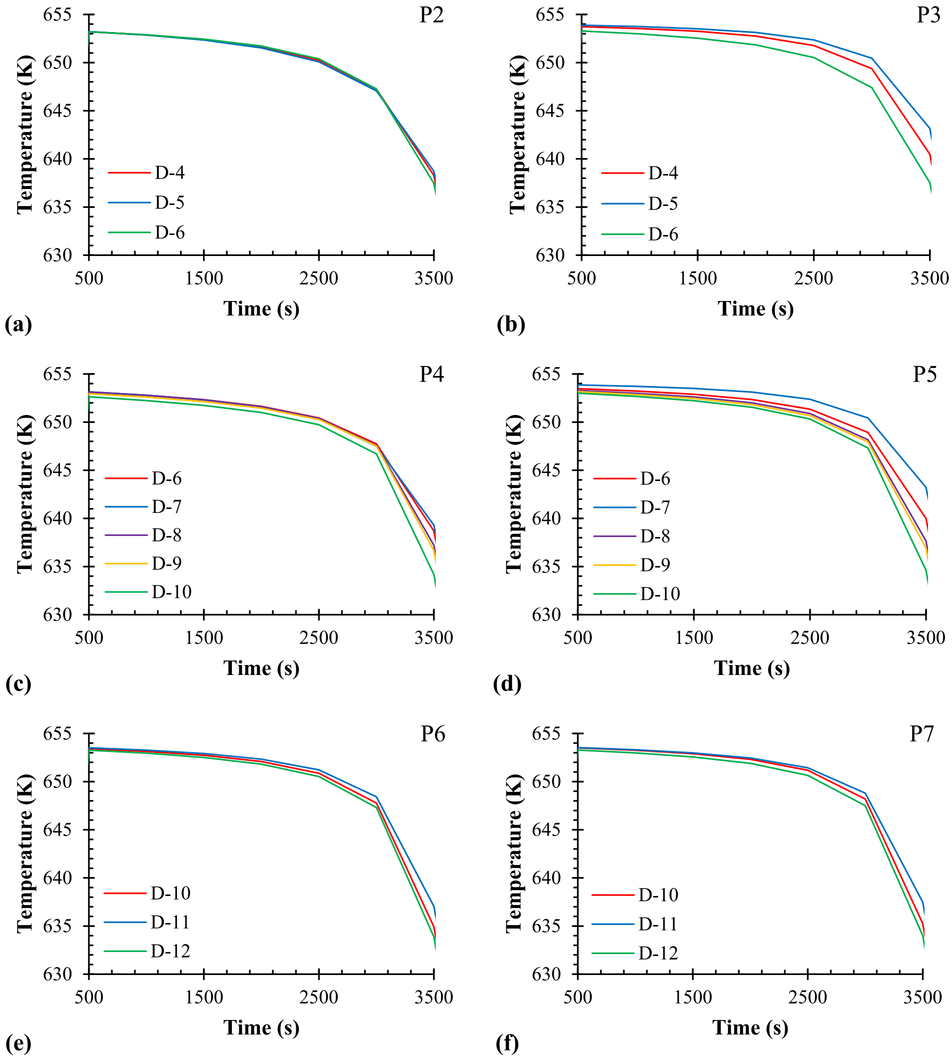

Fig. 11. Temperature at selected point based on the influences of fin angle, fin height, and fin width for triple-branched section (from case D-4 to case D-6, case D-6 to case D-10, and from case D-10 to case D-12); (a) at P2, (b) at P3, (c) at P4, (d) at P5, (e) at P6, and (f) at P7.

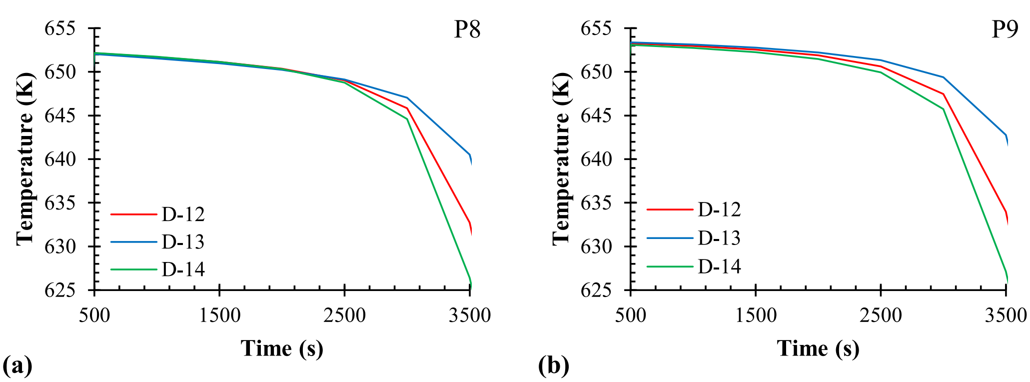

Fig. 12. Temperature at selected point based on the influence of fin thickness at first and third branches (from case D-12 to case D-14); (a) at P8 and (b) at P9.

hydrogen concentration as this area is close to the HTF tube. Other areas close to the fin also have a higher hydrogen concentration, but this concentration is still lower than the central area. It is obvious that case D-14 obtains a faster hydrogen absorption as this case always has a higher hydrogen concentration, especially around the fin domain. At 3500 s, there is full hydrogen absorption (100 % concentration) from case D-14, where it is still at 81 % concentration from some areas in the middle and the top corner areas of the MHHS from case D. The hydrogen concentration contours from Fig. 13 prove that the fin angle, fin width, and fin height of the triple-branched fin, significantly affect the heat transfer mechanism, leading to a faster hydrogen kinetic reaction.

4.3.4. *Influence of fin designs on hydrogen absorption-desorption cycle*

The comparison of the hydrogen absorption-desorption cycle based

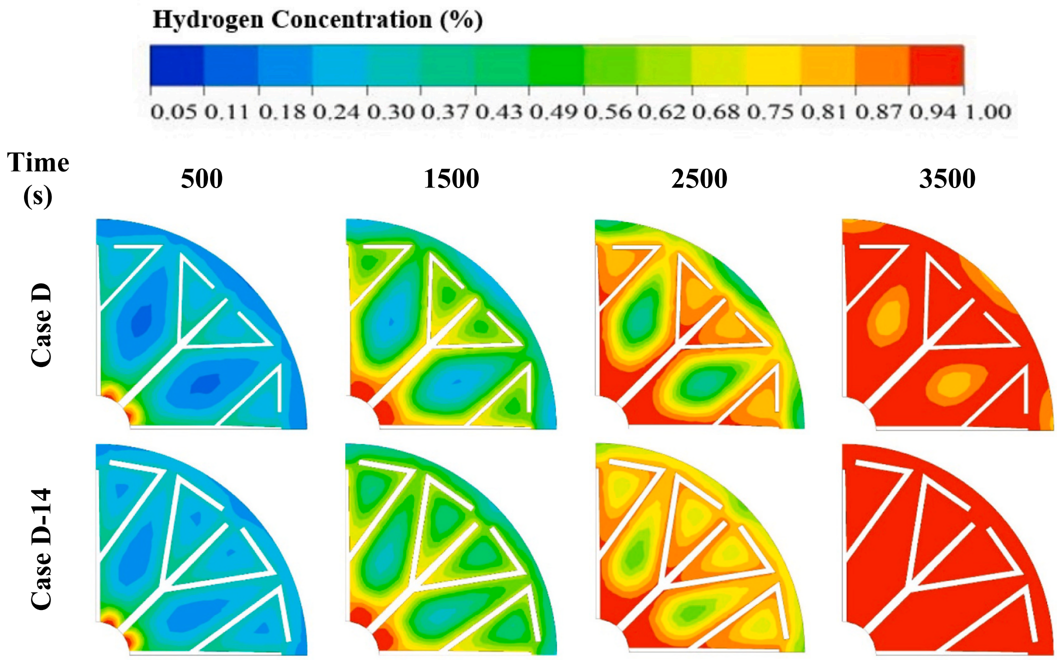

Fig. 13. Hydrogen concentration at 500 s, 1500 s, 2500 s, and 3500 s after starting hydrogen absorption process from case D and case D-14.

on various fin designs is presented in Fig. 14. From this figure, the final times of one complete cycle from case A to case D are 21,047 s, 18675 s, 17440 s, and 16,782 s, respectively. Considering the reduction of absorption-desorption duration from case A (as the base case), there are 11 % reduction from case B, 17 % reduction from case C, and 20 % reduction from case D. After the development of case D, the duration of one complete cycle from case D-14 is only 15,869 s, which is less than 16,000 s. Comparing to case A, case D-14 obtains a 25 % reduction of one complete cycle. Considering the volumetric and gravimetric of the MHHS, these two are the main factors for the compact MHHS [32]. The weight of heat exchangers should be optimised for the use of compact MHHS, such as automobile applications. To achieve a reasonable driving range, the MHHS must suit the size of the vehicle without adding too much weight [32]. Focusing on the MH volume from case D-14, it has only a 10 % reduction of MH volume when comparing with case A. There is only a 20 % reduction in MH volume compared to the MHHS without any heat exchangers. Therefore, it is obvious that the new fin design (case D), especially after the development (case D-14), obtains better heat transfer mechanisms compared to the original fin design as a straight-shaped fin and a Y-shaped fin. Therefore, case D-14 is then selected for further analysis of its performance under the parametric study section. Focusing on the reduction of absorption and desorption duration from Fig. 14b, the development of fin design is more effective in the hydrogen kinetic reaction during the hydrogen absorption rather

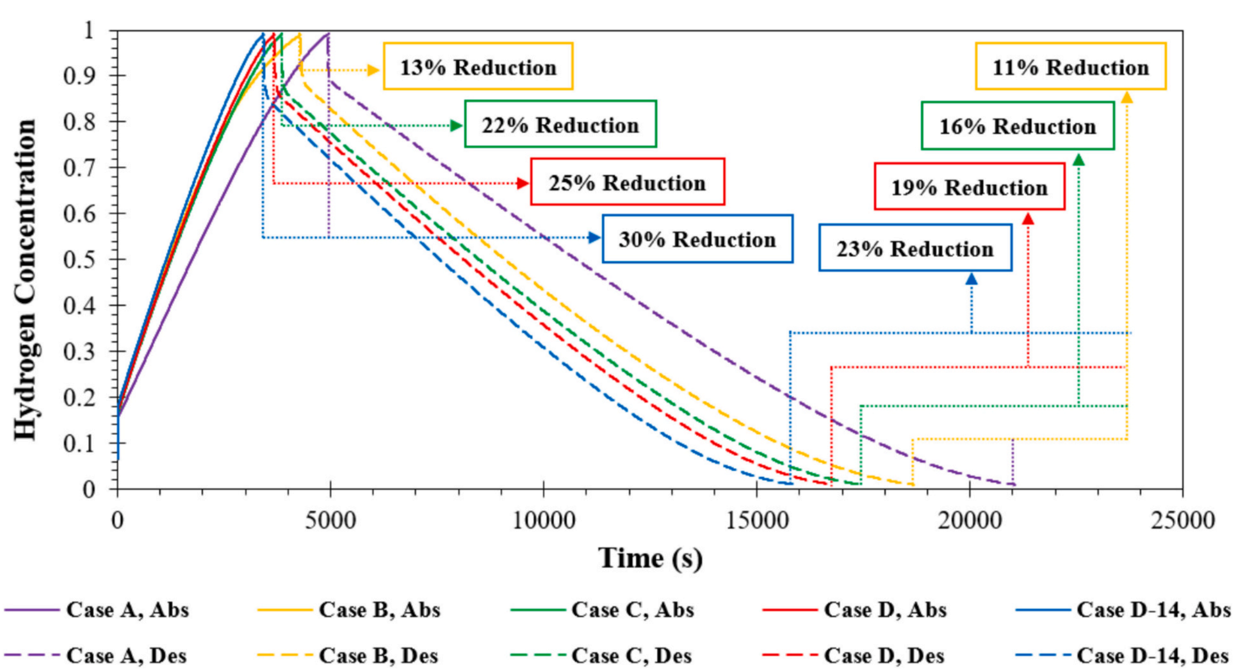

Fig. 14. Average hydrogen concentration for hydrogen absorption-desorption cycle from various fin designs.

than the hydrogen desorption. This is obvious in the reduction percentage from each case. However, this is only applied in the case of having the same HTF temperature as 573 K for both processes. Selecting a higher HTF temperature for the hydrogen desorption can cause faster hydrogen desorption. The effect of various initial HTF temperatures is then analysed and presented under the parametric study.

Furthermore, the results from case D-14 prove that this case, which contains the straight tube and triple-branched fins, obtains better heat transfer efficiency and shorter hydrogen absorption/desorption duration. The hydrogen absorption-desorption duration from this case is less than 16,000 s, while the final time from the SCHE-CR is 17,270 s. It should be noted that there is a 15 % increase in heat exchanger volume when using the design from case D-14, compared to the SCHE-CR case. This results in a reduction of MH volume from case D-14. In contrast, there is only 3 % pressure loss from the case with a straight tube, while there is over 34 % pressure loss from the case with coil tubes. However, the difference in hydrogen absorption-desorption duration from these two cases is because of the difference in material use of each heat exchanger. The material used for SCHE-CR is stainless steel, which offers a low thermal conductivity, compared to other materials. The material used in all fin designs in this study is copper, which offers a high thermal conductivity. These can cause a major difference in heat transfer performance. Under the use of stainless steel as the SCHE-CR material, this material was selected at the beginning from our previous studies due to its advantages, which offer more resistance in damage and superior corrosion resistance. It is worth mentioning that this present study only focuses on the fin geometric design and its performance. The comparison between the use of different heat exchanger materials for SCHE-CR and others are not considered in this study.

4.4. Parametric study for operating conditions

The parametric study in this study focuses on three operating parameters. The MHHS temperature is set as 573 K for all cases of hydrogen absorption, while the initial MHHS temperature for the desorption is set as the ultimate temperature at the end of the absorption process. The loading pressure is set as 1.8 MPa during hydrogen absorption, whereas the pressure of 0.1 MPa is used for hydrogen desorption.

4.4.1. Heat transfer fluid temperature

The initial HTF temperature plays a significant role in the improvement of the hydrogen kinetic reaction during absorption/desorption. Reducing the HTF temperature obtains faster hydrogen absorption as the MHHS must be cooled down during this stage. In contrast, the MHHS must be heated up for faster hydrogen desorption purposes. In general, the range of temperature for hydrogen absorption and desorption are varied depending on the MH materials [59]. Therefore, the choice of HTF is based on the selected MH material [59]. From our present study, air is selected as the HTF due to the high operating temperature range of magnesium-based alloy [54]. Fig. 15 presents the effect of various HTF temperatures during the hydrogen absorption/desorption. The heat transfer coefficient between the HTF and MH bed is set as 500 W m^{-2} K^{-1} for all cases. From Fig. 15a, a greater reduction of initial HTF temperature obtains faster hydrogen absorption. The absorption durations from these cases are 3427 s for 573 K, 2164 s for 523 K, 1595 s for 473, and 1271 s for 423 K. Comparing to the base value of 573 K, there is a 37–63 % reduction of the absorption time when the temperature decreases from 573 K to 423 K. From Fig. 15b, increasing the HTF temperature significantly reduces the hydrogen desorption duration. The hydrogen desorption durations from these cases are 12,442 s for 573 K, 4717 s for 623 K, 2917 s for 673 K, and 2115 s for 723 K. Comparing to the base HTF temperature at 573 K, there is a 62–83 % reduction of hydrogen desorption duration when increasing the HTF temperature from 573 K to 723 K. It can be seen that changing the HTF temperature significantly affects the hydrogen kinetic reaction rate, especially during the desorption process. The initial HTF temperature during the desorption process should be higher than 623 K.

4.4.2. Heat transfer coefficient between heat transfer fluid and metal hydride

This section provides the investigation of the heat transfer coefficient (h_f) between the HTF and MH bed on the heat transfer performance. Fig. 16 indicates the effect of various h_f values on hydrogen absorption (Fig. 16a) and hydrogen desorption (Fig. 16b). The initial HTF temperature is set as 573 K for both hydrogen absorption and desorption. From Fig. 16a, the absorption durations from these cases are 5794 s for 250 W m^{-2} K^{-1}, 3427 s for 500 W m^{-2} K^{-1}, 2602 s for 750 W m^{-2} K^{-1}, and 2167 s for 1000 W m^{-2} K^{-1}. Comparing to the base value at 250 W m^{-2} K^{-1}, there is a 41–63 % reduction of hydrogen absorption duration when increases the h_f value from 250 W m^{-2} K^{-1} to 1000 W m^{-2} K^{-1}. From Fig. 16b, the desorption duration from these cases are 19,415 s for 250 W m^{-2} K^{-1}, 12,442 s for 500 W m^{-2} K^{-1}, 9985 s for 750 W m^{-2} K^{-1}, and 8685 s for 1000 W m^{-2} K^{-1}. Comparing to the base value at 250 W m^{-2} K^{-1}, it obtains a 36–55 % reduction of hydrogen absorption duration when increases the h_f value from 250 W m^{-2} K^{-1} to 1000 W m^{-2} K^{-1}. In general, the amount of heat transfer in the MH bed is directly proportional to the h_f [44]. Increasing the h_f between the HTF and MH

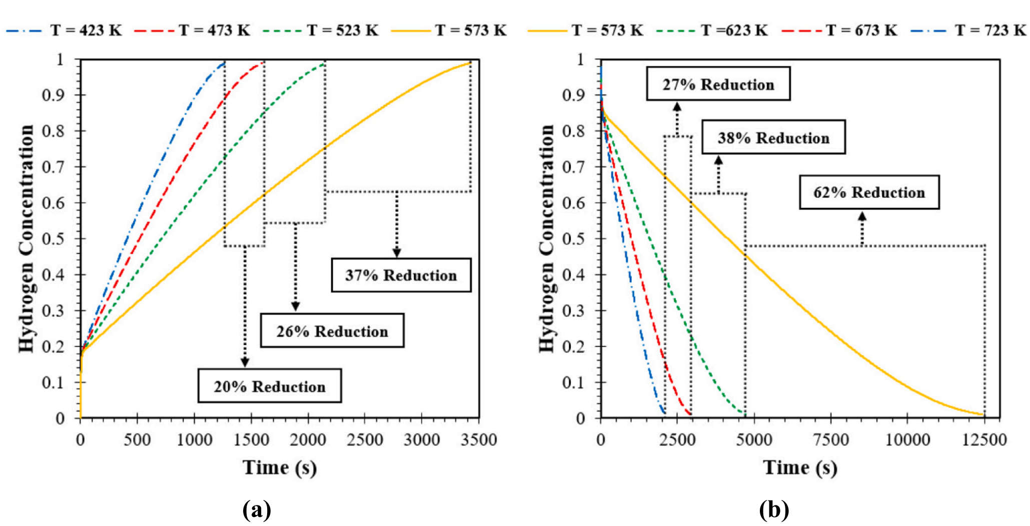

Fig. 15. Hydrogen concentration based on various initial temperatures of HTF from case D-14; (a) during hydrogen absorption and (b) during hydrogen desorption.

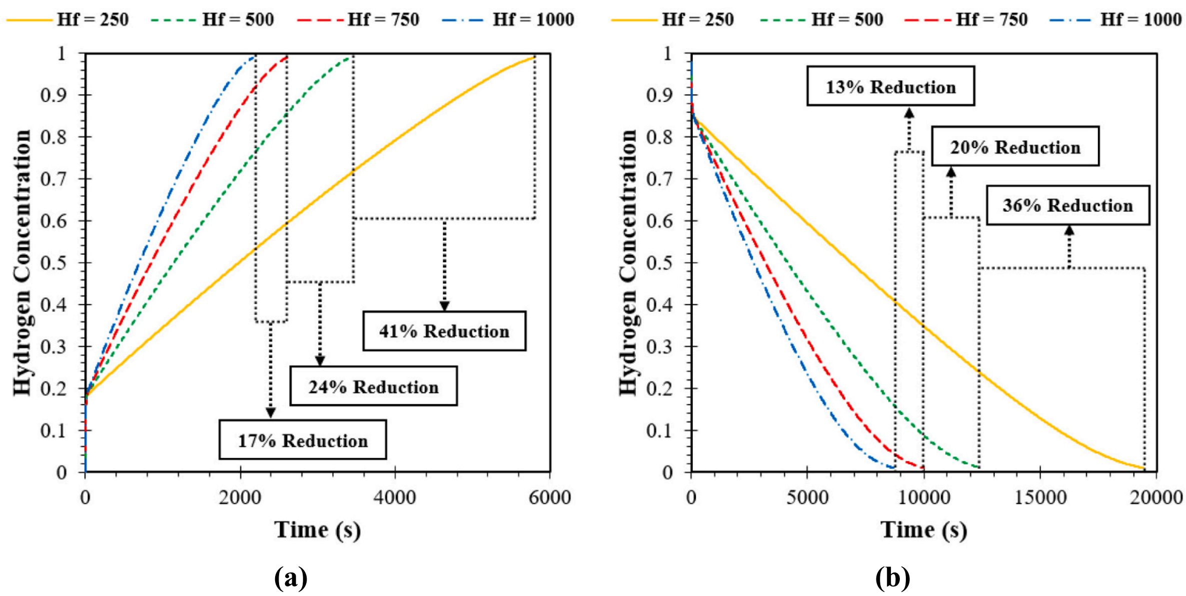

Fig. 16. Hydrogen concentration based on various heat transfer coefficients between HTF and HTF tube from case D-14; (a) during hydrogen absorption and (b) during hydrogen desorption.

bed positively affects the hydrogen kinetic reaction for both hydrogen absorption and desorption processes [44]. This is because of the fast reduction in MH bed temperature during the absorption and the fast increase in MH bed temperature during the desorption. It can be summarised that the h_f has a better effect on hydrogen absorption rather than hydrogen desorption. However, this is only applied to the case when using the initial HTF temperature of 573 K for both absorption and desorption.

4.4.3. Material used for heat exchanger tube and fin

Appropriate selecting material for the heat exchanger tube and fin also plays a significant role in heat transfer management. Four different materials are selected and analysed for their performances under hydrogen absorption and desorption, which are presented in Fig. 17. These four materials include copper, aluminum, nickel, and steel. For all cases, the initial temperature of the HTF and the h_f between the HTF and MH bed are set as 573 K and 500 W m^{-2} K^{-1}. In general, thermal efficiency, cost, corrosion resistance, compatibility fabrication, and durability are general factors, that should be considered when choosing material for heat exchanger purposes. The material should have a high thermal conductivity to offer more effective to conduct and transfer heat [60]. When using the material with a high thermal conductivity of the HTF tube and fin, the heat transfer efficiency is much higher, compared to the material with low thermal conductivity. From Fig. 17, it can be seen that steel obtains the longest time to complete the hydrogen absorption and desorption processes. The final time for the hydrogen absorption-desorption cycle based on steel is 21,697 s. However, the final time for one cycle from other materials is less than 17,000 s as these materials have a higher thermal conductivity compared to steel (refer to Table 4 for thermal-physical properties of each material). The final time for one cycle based on nickel, aluminum, and copper is 16,748 s, 16265 s, and 15,869 s, respectively. A higher thermal conductivity causes a

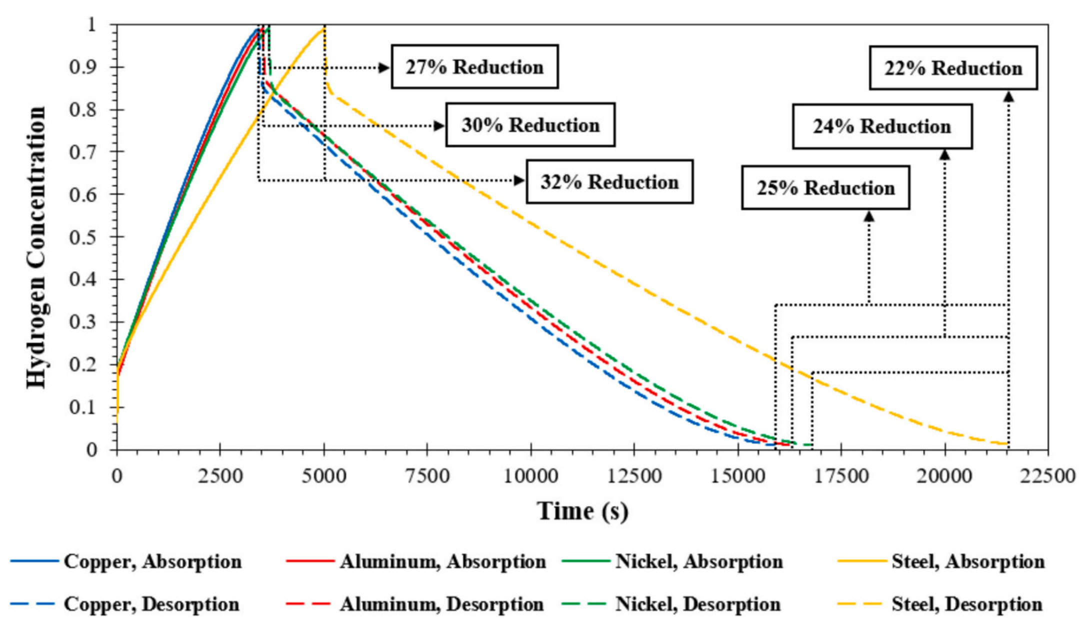

Fig. 17. Hydrogen concentration during absorption-desorption cycle based on various materials of HTF tube and fin from case D-14.

shorter time to complete the hydrogen absorption-desorption cycle. This is because the greater heat transfer efficiency significantly affects the hydrogen kinetic reaction as the faster heat reduction results in a faster hydrogen absorption, while the faster heat addition leads to faster hydrogen desorption [52]. Therefore, the duration of one complete cycle from nickel, aluminum, and copper reduces by 23–27 % when compared to the case with steel. However, copper obtains faster hydrogen absorption/desorption, compared to other materials. This is because the thermal diffusivity and effusivity of copper are better than other materials [61]. When considering the hydrogen absorption-desorption duration from the new fin design, nickel, aluminum, and copper are recommended to be used as the material of the HTF tube and fin. The difference in hydrogen absorption-desorption duration between these three materials is less than 5 %. However, it should be noted that this study only considers the thermal performance of heat exchanger based on thermal conductivity from different materials and its effect on the hydrogen absorption-desorption duration. Other factors, such as cost, compatibility fabrication, and durability, are not considered in this study.

5. Conclusion

The present study proposes a new MHHS configuration incorporating a cooling tube and fin heat exchanger. The simple straight tube is used as a cooling tube instead of other complex heat exchangers to maintain the pressure level. The effect of pressure loss due to the complex HTF tube's structure is investigated to support the selection of a cooling tube to integrate with the new fin design. The novel triple-branched fin design is proposed to fulfil the requirement of heat transfer efficiency instead of using the complex HTF tube. The fin geometry is analysed by considering the increase in heat transfer surface area and fin mass distribution. Various fin designs are also proposed in this study to compare the fin performance under the average MH bed temperature and hydrogen absorption/desorption. Furthermore, the overall MH bed volumes before and after enhancing the fin performance are also investigated in this study. In the parametric study during hydrogen absorption and desorption, the three main selected parameters include the effect of various initial HTF temperatures, the influence of the heat transfer coefficient between the HTF and MH, and the effect of different materials of the fin and HTF tube. The key findings are summarised in the following points:

- There is a 3 % pressure loss from the inlet throughout the outlet of the straight tube heat exchanger, while there is over a 34 % pressure loss throughout the coil heat exchangers.
- Under four different fin designs, the MHHS with the novel triple-branched fin obtains the best performance with a 25 % reduction of absorption duration and less than a 5 % reduction of the MH volume, compared to the case with a quadrilateral fin.
- After enhancing the fin performance, the durations of absorption and desorption are reduced by 30 % and 23 %, compared to the case with quadrilateral fin. For one complete cycle, the duration for this complete cycle from the triple-branched fin after the enhancement is reduced by 25 %, compared to the conventional quadrilateral fin. Due to the complex fin structure, which obtains more fin distribution inside the MHHS, there is more uniform temperature distribution along the MH bed and lower thermal resistance. This results in a faster hydrogen kinetic reaction. In other words, it results in faster hydrogen absorption/desorption.
- Considering the MH volume reduction, the fin height and width of the triple-branched section, as well as the fin angle at the top branches, are the key parameters to increase the heat transfer efficiency.
- The HTF temperature for the new MHHS configuration significantly affects the MHHS performance, especially for the hydrogen desorption process. The absorption duration reduces by up to 63 % when the HTF temperature is reduced from 573 K to 423 K. However, the desorption duration further reduces by up to 83 % when the HTF temperature increases from 573 K to 723 K.
- The heat transfer coefficient between the HTF and MH bed has a more positive effect on the hydrogen absorption process rather than the hydrogen desorption process with up to 63 % reduction of absorption duration and up to 55 % reduction of desorption when changing the heat transfer coefficient from 250 W m^{-2} K^{-1} to 1000 W m^{-2} K^{-1}.
- Using steel as the fin and HTF tube material obtains less effect on the hydrogen absorption/desorption, compared to other materials, including nickel, aluminum, and copper. The duration of one complete cycle from these materials is 23–27 % less than the case with steel.

This study proposes a new magnesium-based hydrogen storage configuration incorporating the internal fin with the cooling tube. The comprehensive investigation of this new configuration on the heat transfer performance and the hydrogen kinetic reaction during the hydrogen absorption/desorption process, is also provided in this study. Furthermore, the effect of fin geometry based on the selected fin parameters is analysed under the temperature variation along the metal hydride bed. It should be noted that the purpose of this study is to introduce the novel triple-branched fin design with the use of a simple cooling tube. The effect of fin parameters on the heat transfer improvement is performed by basic investigations. More analysis of the novel fin design will be considered in future studies by focusing on the effect of different fin ratios, such as fin length, fin width, and fin angle, on the heat transfer enhancement and fin efficiency. Moreover, the future studies will also focus on the fin structure and its strength to withstand the impact of the hydride. To avoid lengthy analog computation for multi-parameter studies, the intelligent algorithms such as artificial neural network (ANN) will be considered in future studies. However, experiment studies regarding this storage configuration are required to obtain concrete, practical results and ensure that this configuration can be applied to industrial settings and supported advancements in hydrogen storage applications.

CRediT authorship contribution statement

Puchanee Larpruenrudee: Writing – original draft, Validation, Software, Resources, Methodology, Formal analysis, Data curation, Conceptualization. **Nick S. Bennett:** Writing – review & editing, Supervision, Conceptualization. **Robert Fitch:** Writing – review & editing, Supervision, Conceptualization. **Emilie Sauret:** Writing – review & editing. **YuanTong Gu:** Writing – review & editing. **M.J. Hossain:** Writing – review & editing. **Mohammad S. Islam:** Writing – review & editing, Supervision, Resources, Conceptualization.

Declaration of competing interest

The authors declare that they have no known competing financial interests or personal relationships that could have appeared to influence the work reported in this paper.

Acknowledgements

The authors acknowledge the high-performance computing facility at the University of Technology Sydney.

Data availability

Data will be made available on request.

References

[1] M. Eslami, F. Khosravi, H.R. Fallah Kohan, Effects of fin parameters on performance of latent heat thermal energy storage systems: a comprehensive review, Sustain. Energy Technol. Assess. 47 (2021) 101449, https://doi.org/10.1016/j.seta.2021.101449.

[2] Y. Zhang, A. Faghri, Heat transfer enhancement in latent heat thermal energy storage system by using the internally finned tube, Int. J. Heat Mass Transf. 39 (15) (1996) 3165–3173, https://doi.org/10.1016/0017-9310(95)00402-5.

[3] C.R.E.S. N'obrega, K.A.R. Ismail, F.A.M. Lino, Enhancement of ice formation around vertical finned tubes for cold storage applications, Int. J. Refrig. 99 (2019) 251–263, https://doi.org/10.1016/j.ijrefrig.2018.12.018.

[4] S. Lohrasbi, M. Sheikholeslami, D.D. Ganji, Discharging process expedition of NEPCM in fin-assisted latent heat thermal energy storage system, J. Mol. Liq. 221 (2016) 833–841, https://doi.org/10.1016/j.molliq.2016.06.044.

[5] A. Sciacovelli, F. Gagliardi, V. Verda, Maximization of performance of a PCM latent heat storage system with innovative fins, Appl. Energy 137 (2015) 707–715, https://doi.org/10.1016/j.apenergy.2014.07.015.

[6] S. Lohrasbi, M.G. Bandpy, D.D. Ganji, Response surface method optimization of V-shaped fin assisted latent heat thermal energy storage system during discharging process, Alex. Eng. J. 55 (3) (2016) 2065–2076, https://doi.org/10.1016/j.aej.2016.07.004.

[7] K. Hosseinzadeh, M. Alizadeh, D.D. Ganji, Solidification process of hybrid nanoenhanced phase change material in a LHTESS with tree-like branching fin in the presence of thermal radiation, J. Mol. Liq. 275 (2019) 909–925, https://doi.org/10.1016/j.molliq.2018.11.109.

[8] M. Sheikholeslami, R. Haq, A. Shafee, Z. Li, Y.G. Elaraki, I. Tlili, Heat transfer simulation of heat storage unit with nanoparticles and fins through a heat exchanger, Int. J. Heat Mass Transf. 135 (2019) 470–478, https://doi.org/10.1016/j.ijheatmasstransfer.2019.02.003.

[9] B. Sakintuna, F. Lamari-Darkrim, M. Hirscher, Metal hydride materials for solid hydrogen storage: a review, Int. J. Hydrog. Energy 32 (9) (2007) 1121–1140, https://doi.org/10.1016/j.ijhydene.2006.11.022.

[10] I. Jain, C. Lal, A. Jain, Hydrogen storage in Mg: a most promising material, Int. J. Hydrog. Energy 35 (10) (2010) 5133–5144, https://doi.org/10.1016/j.ijhydene.2009.08.088.

[11] W. Zhao, Y. Yang, Z. Bao, Y. Dong, Z. Zhu, Methods for measuring the effective thermal conductivity of metal hydride beds: a review, Int. J. Hydrog. Energy 45 (11) (2020) 6680–6700, https://doi.org/10.1016/j.ijhydene.2019.12.185.

[12] V. Keshari, M.P. Maiya, Design and investigation of hydriding alloy based hydrogen storage reactor integrated with a pin fin tube heat exchanger, Int. J. Hydrog. Energy 43 (14) (2018) 7081–7095, https://doi.org/10.1016/j.ijhydene.2018.02.100.

[13] P. Muthukumar, A. Singhal, G. Bansal, Thermal modeling and performance analysis of industrial-scale metal hydride based hydrogen storage container, Int. J. Hydrog. Energy 37 (19) (2012) 14351–14364, https://doi.org/10.1016/j.ijhydene.2012.07.010.

[14] K.B. Krishna, P.K. Kanti, M.P. Maiya, A novel fin efficiency concept to optimize solid state hydrogen storage reactor, Energy 288 (2024) 129789, https://doi.org/10.1016/j.energy.2023.129789.

[15] K.B. Krishna, P.K. Kanti, M.P. Maiya, Design optimization of metal hydride-based hydrogen storage reactor using fin efficiency concept, in: 38th ISTANBUL International Conference on Advances in "Science, Engineering & Technology" (IASET-24) May 13–15, 2024 Istanbul (Turkiye), 2024.

[16] J. Ma, Y. Wang, S. Shi, F. Yang, Z. Bao, Z. Zhang, Optimisation of heat transfer device and analysis of heat & mass transfer on the finned multi-tubular metal hydride tank, Int. J. Hydrog. Energy 39 (25) (2014) 13583–13595, https://doi.org/10.1016/j.ijhydene.2014.03.016.

[17] A. Mallik, P. Sharma, Modeling and numerical simulation of an industrial scale metal hydride reactor based on CFD-Taguchi combined method, Energy Storage 3 (3) (2021) 227, https://doi.org/10.1002/est2.227.

[18] X.S. Bai, W.W. Yang, X.Y. Tang, F.S. Yang, Y.H. Jiao, Y. Yang, Optimisation of tree-shaped fin structures towards enhanced absorption performance of metal hydride hydrogen storage device: a numerical study, Energy 220 (2021) 119738, https://doi.org/10.1016/j.energy.2020.119738.

[19] I. Ayub, M.S. Nasir, Y. Liu, A. Munir, Z. Wu, F. Yang, Z. Zhang, Numerical modeling and performance comparison of high-temperature metal hydride reactor equipped with bakery system for solar thermal energy storage, Int. J. Hydrog. Energy 45 (56) (2020) 31612–31631, https://doi.org/10.1016/j.ijhydene.2020.08.206.

[20] A. Singh, M.P. Maiya, S.S. Murthy, Performance of a solid state hydrogen storage device with finned tube heat exchanger, Int. J. Hydrog. Energy 42 (43) (2017) 26855–26871, https://doi.org/10.1016/j.ijhydene.2017.06.071.

[21] X.S. Bai, W.W. Yang, W.Y. Zhang, F.S. Yang, X.Y. Tang, Hydrogen absorption performance of a novel cylindrical MH reactor with combined loop-type finned tube and cooling jacket heat exchanger, Int. J. Hydrog. Energy 45 (52) (2020) 28100–28115, https://doi.org/10.1016/j.ijhydene.2020.04.209.

[22] H. Dhaou, N.B. Khedher, S. Mellouli, A. Souahlia, F. Askri, A. Jemni, S.B. Nasrallah, Improvement of thermal performance of spiral heat exchanger on hydrogen storage by adding copper fins, Int. J. Therm. Sci. 50 (12) (2011) 2536–2542, https://doi.org/10.1016/j.ijthermalsci.2011.05.016.

[23] A. Souahlia, H. Dhaou, S. Mellouli, F. Askri, A. Jemni, S.B. Nasrallah, Experimental study of metal hydride-based hydrogen storage tank at constant supply pressure, Int. J. Hydrog. Energy 39 (14) (2014) 7365–7372, https://doi.org/10.1016/j.ijhydene.2014.02.121.

[24] S. Mellouli, F. Askri, H. Dhaou, A. Jemni, S.B. Nasrallah, Numerical simulation of heat and mass transfer in metal hydride hydrogen storage tanks for fuel cell vehicles, Int. J. Hydrog. Energy 35 (4) (2010) 1693–1705, https://doi.org/10.1016/j.ijhydene.2009.12.052.

[25] K.V. Krisha, P.K. Kanti, M.P. Maiya, A novel flat coil heat exchanger for metal hydride hydrogen storage reactors, Int. J. Hydrog. Energy 64 (2024) 98–108, https://doi.org/10.1016/j.ijhydene.2024.03.063.

[26] A.P. Shtivastav, P.K. Kanti, G. Mohan, M.P. Maiya, Design and optimization of metal hydride reactor with phase change material using fin factor for hydrogen storage, J. Energy Storage 77 (2024) 109975, https://doi.org/10.1016/j.est.2023.109975.

[27] F. Guan, W. Ma, Y. Tu, C. Zhou, B. Zhou, An experimental study of flow behavior of coiled tubing drilling system, Adv. Mech. Eng. 6 (2014), https://doi.org/10.1155/2014/935159.

[28] Z. Zhang, H. Liu, Research on the thermal performance of a helical coil heat exchanger, in: Proceedings of the International Conference of Fluid Power and Mechatronic Control Engineering, Atlantis Highlights in Engineering, 2022, December 7, https://doi.org/10.2991/978-94-6463-022-0_11.

[29] C.S. Wang, J. Brinjerhoff, Is there a general time scale for hydrogen storage with metal hydrides or activated carbon? Int. J. Hydrog. Energy 46 (2021) 12031–12034, https://doi.org/10.1016/j.ijhydene.2021.01.067.

[30] C.S. Wang, J. Brinjerhoff, Predicting hydrogen adsorption and desorption rates in cylindrical metal hydride beds: empirical correlations and machine learning, Int. J. Hydrog. Energy 46 (2021) 24256–24270, https://doi.org/10.1016/j.ijhydene.2021.05.007.

[31] L. Klebanoff, L. Klebanoff, Hydrogen Storage Technology: Materials and Applications, 1st edition, CRC Press, 2012, https://doi.org/10.1201/b13685.

[32] A. Rahnama, G. Zepon, S. Sridhar, Machine learning based prediction of metal hydrides for hydrogen storage, part I: prediction of hydrogen weight percent, Int. J. Hydrog. Energy 44 (2019) 7337–7344, https://doi.org/10.1016/j.ijhydene.2019.01.261.

[33] S. Yao, X. Huang, Study on solidification performance of PCM by longitudinal triangular fins in a triplex-tube thermal energy storage system, Energy 227 (2021) 102527, https://doi.org/10.1016/j.energy.2021.120527.

[34] A. Hickie-Bentzen, M. Elsharqawy, S.H. Tasnim, S. Mahmud, Parametric investigation of internal Y-shaped fin configurations under natural convection in a concentric annulus, Results Eng. 16 (2022) 100692, https://doi.org/10.1016/j.rineng.2022.100692.

[35] S. Zhang, S. Mancin, L. Pu, A review and prospective of fin design to improve heat transfer performance of latent thermal energy storage, J. Energy Storage 62 (2023) 106825, https://doi.org/10.1016/j.est.2023.106825.

[36] P. Larpruenrudee, N.S. Bennett, Z. Luo, R. Fitch, E. Sauret, M.S. Islam, A novel design for faster hydrogen storage: a combined semi-cylindrical and central return tube heat exchanger, J. Energy Storage 71 (2023) 108018, https://doi.org/10.1016/j.est.2023.108018.

[37] P. Larpruenrudee, N.S. Bennett, R. Fitch, E. Sauret, Y.T. Gu, M.S. Islam, Investigation of metal hydride hydrogen storage performance using phase change materials, Int. J. Hydrog. Energy 60 (2024) 996–1019, https://doi.org/10.1016/j.ijhydene.2024.02.057.

[38] B.S. Sekhar, M. Lototskyy, A. Kolesnikov, M.L. Moropeng, B. Tarasov, B. Pollet, Performance analysis of cylindrical metal hydride beds with various heat exchange options, J. Alloys Compd. 645 (2015) S89–S95, https://doi.org/10.1016/j.jallcom.2014.12.272.

[39] C. Chung, C.S. Lin, Prediction of hydrogen desorption performance of Mg2Ni hydride reactors, Int. J. Hydrog. Energy 34 (23) (2009) 9409–9423, https://doi.org/10.1016/j.ijhydene.2009.09.061.

[40] A. Chaise, P. Marty, P. de Rango, D. Fruchart, A simple criterion for estimating the effect of pressure gradients during hydrogen absorption in a hydride reactor, Int. J. Heat Mass Transf. 52 (19–20) (2009) 4564–4572, https://doi.org/10.1016/j.ijheatmasstransfer.2009.03.052.

[41] A. Jemni, S.B. Nasrallah, J. Lamloumi, Experimental and theoretical study of a metal–hydrogen reactor, Int. J. Hydrog. Energy 24 (7) (1999) 631–644, https://doi.org/10.1016/S0360-3199(98)00117-7.

[42] A. Chaise, P. De Rango, P. Marty, D. Fruchart, Experimental and numerical study of a magnesium hydride tank, Int. J. Hydrog. Energy 35 (12) (2010) 6311–6322, https://doi.org/10.1016/j.ijhydene.2010.03.057.

[43] M. Valizadeh, M.A. Delavar, M. Farhadi, Numerical simulation of heat and mass transfer during hydrogen desorption in metal hydride storage tank by lattice Boltzmann method, Int. J. Hydrog. Energy 41 (1) (2016) 413–424, https://doi.org/10.1016/j.ijhydene.2015.11.075.

[44] A.H. Eisapour, A. Naghizadeh, M. Eisapour, P. Talebizadehsardari, Optimal design of a metal hydride hydrogen storage bed using helical coil heat exchanger along with a central return tube during the absorption process, Int. J. Hydrog. Energy 46 (2021) 14478–14493, https://doi.org/10.1016/j.ijhydene.2021.01.170.

[45] Z. Wu, F. Yang, L. Zhu, P. Feng, Z. Zhang, Y. Wang, Improvement in hydrogen desorption performances of magnesium based metal hydride reactor by incorporating helical coil heat exchanger, Int. J. Hydrog. Energy 41 (36) (2016) 16108–16121, https://doi.org/10.1016/j.ijhydene.2016.04.224.

[46] Z. Bao, F. Yang, Z. Wu, X. Cao, Z. Zhang, Simulation studies on heat and mass transfer in high-temperature magnesium hydride reactors, Appl. Energy 112 (2013) 1181–1189, https://doi.org/10.1016/j.apenergy.2013.04.053.

[47] P. Muthukumar, M. Prakash Maiya, S. Srinivasa Murthy, R. Vijay, R. Sundaresan, Tests on mechanically alloyed Mg2Ni for hydrogen storage, J. Alloys Compd. 452 (2) (2008) 456–461, https://doi.org/10.1016/j.jallcom.2007.03.112.

[48] N.A.A. Rusman, M. Dahari, A review on the current progress of metal hydrides material for solid-state hydrogen storage applications, Int. J. Hydrog. Energy 41 (28) (2016) 12108–12126, https://doi.org/10.1016/j.ijhydene.2016.05.244.

[49] G. Liang, Synthesis and hydrogen storage properties of Mg-based alloys, J. Alloys Compd. 370 (1–2) (2004) 123–128, https://doi.org/10.1016/j.jallcom.2003.09.031.

[50] Z. Wu, F. Yang, Z. Zhang, Z. Bao, Magnesium based metal hydride reactor incorporating helical coil heat exchanger: simulation study and optimal design, Appl. Energy 130 (2014) 712–722, https://doi.org/10.1016/j.apenergy.2013.12.071.

[51] S. Mellouli, E. Abhilash, F. Askri, S.B. Nasrallah, Integration of thermal energy storage unit in a metal hydride hydrogen storage tank, Appl. Therm. Eng. 102 (2016) 1185–1196, https://doi.org/10.1016/j.applthermaleng.2016.03.116.

[52] S.S. Ardahaie, M.J. Hosseini, M. Eisapour, A.H. Eisapour, A.A. Ranjbar, A novel porous metal hydride tank for hydrogen energy storage and consumption assisted by PCM jackets and spiral tubes, J. Clean. Prod. 311 (2021) 127674, https://doi.org/10.1016/j.jclepro.2021.127674.

[53] S.M. Yang, W.Q. Tao, Heat Transfer Theory, 3rd ed., Chinese Higher Education Press, Beijing, 1998.

[54] P. Larpruenrudee, N.S. Bennett, Y.T. Gu, R. Fitch, M.S. Islam, Design optimization of a magnesium-based metal hydride hydrogen energy storage system, Sci. Rep. 12 (2022) 13436, https://doi.org/10.1038/s41598-022-17120-3.

[55] P. Larpruenrudee, N.S. Bennett, M.J. Hossain, R. Fitch, M.S. Islam, Hydrogen energy storage system: how does the semi-cylindrical helical coil heat exchanger affect metal hydride beds' thermal conductivity? in: C. Lei, B. Thornber, S. Armfield (Eds.), Proceeding of the 23rd Australasian Fluid Mechanics Conference, 2022 (Sydney, Australia).

[56] R. Bird, W. Stewart, E. Lightfoot, Transport Phenomena, 2nd edition, John Wiley and Sons, New York, 2002.

[57] P.A. Ward, C. Corgnale, J.A. Teprovicch, T. Motyka, D. Sheppard, C. Buckley, R. Zidan, Technical challenges and future direction for high-efficiency metal hydride thermal energy storage systems, Appl. Phys. A 122 (2016) 462, https://doi.org/10.1007/s00339-016-9909-x.

[58] Z.H. Low, Z. Qin, F. Duan, A review of fin application for latent heat thermal energy storage enhancement, J. Energy Storage 85 (2024) 111157, https://doi.org/10.1016/j.est.2024.111157.

[59] P.K. Kanti, A.P. Shrivastav, P. Sharma, M.P. Maiya, Thermal performance enhancement of metal hydride reactor for hydrogen storage with graphene oxide nanofluid: model prediction with machine learning, Int. J. Hydrog. Energy 52 (2024) 470–484, https://doi.org/10.1016/j.ijhydene.2023.03.361.

[60] Y.A. Cengel, M.A. Boles, Thermodynamics: An Engineering Approach, 8th edition, McGraw Hill, New York, 2015.

[61] F. Hasnain, M. Irfan, M.M. Khan, L.A. Khan, H.F. Ahmed, Melting performance enhancement of a phase change material using branched fins and nanoparticles for energy storage applications, J. Energy Storage 38 (2021) 102513, https://doi.org/10.1016/j.est.2021.102513.